Personalized microbiotas (counter-)select for antibiotic resistant pathogens

Authors

Michael Knopp[1,#], Sarela Garcia-Santamarina[1,4], Lina Michel[1], Dimitrios Papagiannidis[1], Sophia David[2], Denise M. Selegato[1], Joshua L. C. Wong[3], Nicolai Karcher[1], Gad Frankel[3], Michael Zimmermann[1], Mikhail M. Savitski[1], Athanasios Typas[1,#]

Affiliations

[1]Molecular Systems Biology Unit, European Molecular Biology Laboratory, Heidelberg, Germany

[2]Centre for Genomic Pathogen Surveillance, Pandemic Sciences Institute, University of Oxford, Oxford, United Kingdom

[3]Department of Life Sciences, Imperial College London, London, United Kingdom

[4]current address: Deep Microbiome Metabolomics, Hans-Knöll-Institute, Jena, Germany

Contacts

michael.knopp@embl.de and athanasios.typas@embl.de

Keywords

Antibiotic resistance, microbiome, evolution, *K. pneumoniae*, porins, nutrient competition

Abstract

Antibiotic resistant pathogens are an increasing public health threat, as development of novel therapeutics is outpaced by resistance emergence and dissemination. Approaches to slow down or even revert antibiotic resistance are necessary to maintain efficacy of both existing and new antibiotics. Such approaches exploit the fitness cost of resistance elements, but have largely relied on assessing this cost in laboratory conditions that poorly reflect the native context in which pathogens reside. Here we present a method that allows to investigate the influence of personalized human gut microbiota compositions on the competitive fitness of antibiotic resistant pathogens. Using fecal matter-derived microbiomes we identified a specific community that selected for a carbapenem-resistant *Klebsiella pneumoniae* strain. This selective advantage was due to mutations arising in a LacI-type transcriptional regulator, GlyR, which upregulated expression of the downstream glycoporin GlyP, causing the effect. By deconvoluting the microbiome composition, we identified a focal *E. coli* strain as a central driver of the selection, which was further modulated by other microbiota members. We further demonstrate that the selective advantage was due to carbohydrate competition, and in particular for glycerol-containing compounds. Importantly, *glyR* mutations are under strong positive but conditional selection in clinical *K. pneumoniae* isolates. This implies a reduced competitiveness in other environments, which we experimentally validated *in vitro*. Overall, this study offers a path to identify microbiome-specific interactions that modulate the competitiveness of antibiotic resistant pathogens.

Introduction

The spread of antibiotic-resistant pathogens, combined with the lack of development of novel antibiotics, is a major challenge to modern medicine. In addition to reduced capacities to treat life-threatening infections, the spread of resistance jeopardizes life-saving medical procedures that rely on prophylactic antibiotic treatment, such as chemotherapy or surgical procedures[1]. In 2019 alone approximately five million deaths were associated with antibiotic resistant pathogens[2]. As the spread of resistant pathogens increases, deaths linked to them are expected to increase significantly over the next two decades if no decisive action is taken[3]. Despite the immense health and economic burden imposed by antibiotic resistance, development of novel antibiotics has lagged behind in the decades following the 'golden era of antibiotics' between 1940 to 1960, when most major classes of antibiotics were discovered[4,5]. Many reasons have contributed to this, including both challenges in identifying newly acting compounds and the broken antibiotic market. The result is that hardly any novel antibiotic classes have been introduced in clinical use for decades[4], with some hope that the tide will change with a new antibiotic class entering the market recently[6] and more candidates being in the pipeline[7-9]. Instead, most approved compounds in the last decades have been derivatives of antibiotics already in clinical use and are therefore prone to existing resistance mechanisms[10]. In addition to new antibiotics, the improvement of existing therapies can also help in dealing with the antibiotic crisis. This can be facilitated by exploiting drug synergies[11,12], optimizing drug dosing and delivery[13] or developing inhibitors for resistance determinants[14].

A different path to deal with the antibiotic crisis is to understand how cells develop resistance to them, and find ways to prevent, delay or counter-select this process. For example, many resistance determinants have been shown to cause cross-resistance (or collateral sensitivity) where increase in resistance to antibiotic A leads to increase in resistance (or susceptibility) to antibiotic B[15-18]. Treatment regimens can therefore be tailored to avoid pharmaceuticals that share resistance patterns or to combine drug pairs that lead to collateral sensitivity[19]. Although our current knowledge of drug collateral sensitivity is limited, especially since it depends on the pathogen and resistance mechanism, recent developments have opened ways to systematically identify, quantify and understand such drug relationships[20].

In addition to collateral sensitivity to specific compounds, antibiotic resistance acquisition can come with a 'fitness cost' in different environmental conditions[21]. Knowledge of such conditions opens the door for strategies to counter-select the resistant strain and/or promote its displacement by a susceptible strain[22], which can be treated with the antibiotic. Such strategies are particularly relevant for opportunistic pathogens, as removal of resistance can happen at their benign state, allowing for treatment when/if the bacterium becomes pathogenic. Traditionally, such fitness costs of antibiotic-resistance have been measured under axenic lab conditions by quantifying exponential growth rates or maximum yield. While this approach provides several benefits (high reproducibility, easy automation and low costs) and has been successfully employed for mechanistic studies of the effects of resistance acquisition on cellular physiology[23], it does not capture the complexity of the natural environments where pathogenic bacteria reside and antibiotic intervention takes place. For example, many opportunistic human pathogens reside together with other microbes in our body, where they compete for nutrients and niches[24]. The most prominent such microbial community is the human gut microbiome, which serves both as a reservoir for opportunistic pathogens and antibiotic resistance determinants[25-27]. With its diversity, complexity and multitude of interactions (e.g. from nutritional competition to cross feeding[28,29]), it poses a versatile challenge for the competitiveness of an antibiotic resistant bacterium, and at the same time an opportunity to identify strains, molecules and/or niches that expose the Achilles heel of resistance elements. Yet methods to do this are currently lacking.

Here, we present a method to capture fitness costs of antibiotic resistance within complex gut microbiomes, and use it to characterize the impact of diverse microbiome compositions on the fitness of the human pathogen *Klebsiella pneumoniae* carrying resistance determinants that are pervasive amongst clinical isolates causing hard-to-treat infections worldwide. We identify a specific microbiota that selects for the antibiotic-resistant isolate to evolve mutations in a LacI-type transcriptional regulator, which gives the strain a competitive advantage over its susceptible parent in utilizing glycerol containing sugars. This mutational signature emerges recurrently in clinical isolates, suggesting that the observed selective pressures exist in nature. At the same time, such variants seem to be an evolutionary dead end in clinics, likely due to reduced competitiveness in other environments. Consistently we show that these microbiome dependent selections are accompanied by severe tradeoffs in

107 utilization of other carbohydrates, which can be used for their rapid counter-selection. Overall,
108 this study exemplifies how we can utilize fecal matter derived microbiomes to identify
109 (counter-)selective pressures for resistant pathogens, which are prevalent *in vivo*.
110
111

112 Results

113 **A high-throughput method to quantify resistance-associated fitness costs within gut**
114 **microbiomes**

115 Bacterial fitness is typically determined by growth curve assays in axenic conditions or by
116 competition assays where the change in ratio of two competing strains is determined over
117 several passages[30]. The pairwise competition assays are more sensitive and can detect
118 interaction-dependent selective effects that are missed in monocultures. We decided to adapt
119 the classical pairwise-competition assay so it could be performed within a complex microbial
120 community setting, and assess how diverse microbiomes impact the competition of the two
121 focal strains (Fig. 1a, b; Methods).
122

123 We chose *K. pneumoniae* as our model strain due to its classification as a priority human
124 pathogen[2,31], which is frequently associated with antibiotic resistance in clinical settings[32]. *K.*
125 *pneumoniae* is also a common member of the human gut microbiome[33], well studied, easy to
126 cultivate and genetically manipulate. We used a previously characterized isogenic set of *K.*
127 *pneumonia*e strains, which were chromosomally tagged with GFP or RFP markers to allow for
128 sensitive quantification with flow cytometry, and carried antibiotic resistance determinants
129 with minimal fitness effects during axenic growth in nutrient rich conditions[34]. These
130 comprised chromosomal mutations resulting in a loss-of-function deletion and pore-size
131 restriction of the two major porins OmpK35 and OmpK36, respectively (hereafter termed *K.*
132 *pneumoniae ompK*^{mut}) (Fig. 1c), and two clinically prevalent antibiotic resistance plasmids
133 encoding the carbapenemases KPC-2 and OXA-48 (pKpQIL-KPC2 and pOXA-48a). We set out
134 to perform pairwise competition assays between different versions of the resistant *K.*
135 *pneumonia*e strain and its susceptible parent, each carrying a different fluorescent marker
136 (and the marker swap; see methods) in different complex microbiota communities.
137

138 To assess different microbial community compositions, we chose nine native microbiomes
139 derived from fecal samples of healthy human adults (Fig. 1d), and one model synthetic
140 community of 21 different bacterial species that are prevalent in the human gastrointestinal
141 tract[35] and can provide colonization resistance to pathogens[36] (Fig. 1e). All communities were
142 stabilized in mGAM broth under anaerobic conditions for 72 hours with daily passaging, before
143 the two *K. pneumoniae* competitors were spiked into the different microbiomes at a 1:1:20
144 ratio and the community mix was passaged anaerobically for 4 days at a 1:1000 dilution every
145 24 hours, allowing for 10 doublings per day on average. After each passage, ratios of the
146 competitors (GFP or RFP positive), and the overall microbiome (untagged) counts, were
147 determined using flow cytometry. Thereby we could calculate the selection coefficients of the
148 competitors, i.e. the fitness effect per cell per generation, as well as the carrying capacity of
149 the different microbiomes for *K. pneumoniae*. Adapting the experimental setup to a 96 well
150 format, and using liquid-handling robots and a plate-based spectral analyzer, allowed us to
151 scale up the number of mutants/microbiomes tested, while maintaining high sensitivity (Fig.
152 1f). The initial total relative abundance of 10% *K. pneumoniae* when the competition coculture
153 was assembled decreased in all conditions by varying magnitudes. Most microbiomes showed
154 a steady decrease across every passage, suggesting that *K. pneumoniae* cannot easily engraft
155 in some of these communities under the nutritional conditions present in mGAM. Abundance
156 stabilized at approximately 3-4% for the microbiomes, MB003 MB005 and MB007, and to <
157 1% for MB009 (Extended Data Fig. 1).
158
159 In the absence of a microbial community, *K. pneumoniae ompK*^{mut} was as fit as the wildtype,
160 whereas acquisition of the pKpQIL-KPC2 and the pOXA-48a plasmid led to a minor fitness cost
161 of roughly 1 and 2%, respectively (Fig. 1g). Most microbiomes did not cause a significant
162 change in the competitiveness of the antibiotic-resistant mutants or led to a slight reduction
163 in the fitness of *K. pneumoniae ompK*^{mut} and of its derivatives carrying the resistance plasmids
164 – strongest effect being 1.3-2% for MB001. In contrast to all other microbiomes, MB003 led
165 to *K. pneumoniae ompK*^{mut} outcompeting its parental susceptible wildtype by about 4% per
166 cell per generation – at least during later passages (Extended Data Fig. 2). The effect was
167 ameliorated by the presence of pKpQIL-KPC2 and pOXA-48a, as those plasmids conferred
168 fitness costs already in the absence of community. In contrast to all other communities, the
169 plasmid carrying variants were not outcompeted by the wildtype in presence of MB003 (Fig.

170 1g). Altogether these results pointed to antibiotic resistance determinants having
171 microbiome-dependent fitness costs, and highlighted a specific effect of MB003 that led to
172 selection of the antibiotic resistant *K. pneumoniae* porin mutant.
173
174 **Microbiome MB003 drives the evolution of a high-fitness variant of the *K. pneumoniae***
175 **porin mutant**
176 The ratio changes in the competition experiments were constant over time across most
177 conditions, indicating stable fitness differences of the competitors throughout the experiment
178 (Extended Data Fig. 2 and 3), and allowing us to calculate selection coefficients (Fig. 1g).
179 However, replicates of the three pairwise competitions (*K. pneumoniae ompK*^{mut}, *K.*
180 *pneumoniae ompK*^{mut} /pOXA48 and *K. pneumoniae ompK*^{mut} /pKPC-2 versus *K. pneumoniae*
181 wild type) showed a large variation in MB003 (Fig. 1g). In fact, *K. pneumoniae ompK*^{mut} was
182 initially outcompeted by the susceptible wildtype in presence of MB003, and only increased
183 in ratio over the wildtype at later passages (Fig. 1h). This trajectory change during competition
184 experiments is indicative of a secondary mutation being selected during the experiment time
185 course that provides a fitness advantage to one of the competitors. To validate that an
186 underlying genetic change was driving the competitive advantage of the porin mutant in
187 MB003, we isolated the *K. pneumoniae ompK*^{mut} clones from the last day of the competition
188 experiment (hereafter termed *K. pneumoniae ompK*^{evo}), and competed them against the
189 wildtype. In line with our hypothesis, we observed a strong and consistent selective advantage
190 of *K. pneumoniae ompK*^{evo} (Fig. 1i) resulting in a fitness advantage of 7-8% per cell per
191 generation over the wildtype (Fig. 1j). The fitness advantage was specific for MB003, as the
192 evolved clones did not outcompete the wildtype in presence or absence of any of the other
193 microbiomes – with the exception of MB008 which resulted in a moderate fitness advantage
194 of 2% per cell per generation over the wildtype (Extended Data Fig. 4). Altogether we show
195 that MB003 provides a distinct selective milieu that drives the evolution of a *K. pneumoniae*
196 *ompK*^{mut} high-fitness variant able to outcompete the parental susceptible wildtype.
197
198 **A resident *E. coli* strain is driving the selection of a *K. pneumoniae* high-fitness resistant**
199 **mutant in microbiome MB003**
200 To determine the causative MB003 community member(s) for the enrichment of *K.*
201 *pneumoniae ompK*^{evo} we performed a metagenomic analysis of all nine fecal-derived

202 microbiomes (Fig. 2a). All microbiomes exhibited similar Shannon diversities, and contained
203 between 200 and 450 molecular operational taxonomic units (mOTUs)[37], with microbiome
204 MB007 having the least and MB001 having the most mOTUs. Strikingly, MB003 which strongly
205 enriched for *K. pneumoniae ompK*^{evo}, showed the most distinct metagenomic profile with a
206 dominance of Prevotellaceae. To identify which member(s) of microbiome MB003 contributed
207 to the selection of the high-fitness *K. pneumoniae ompK*^{evo} mutant, we chemically perturbed
208 MB003 in order to generate 48 subcommunities with reduced microbial complexity and
209 differential species abundances, as measured by 16S rRNA sequencing (see methods). All
210 subcommunities were then diluted in mGAM and inoculated with the *K. pneumoniae*
211 competitor pair, consisting of *ompK*^{wt} and the high-fitness variant *ompK*^{evo}. To exclude, that
212 the different conditions used to enrich the subcommunities affect the fitness of the different
213 *K. pneumoniae* strains, we performed the competition in pure mGAM. In contrast to previous
214 competition experiments we performed the co-culture competition experiment only for one
215 day as prolonged passaging in mGAM (without the subcommunity selective condition) would
216 likely shift the subcommunity composition causing inconsistent selective conditions. While
217 this experimental setup is less sensitive than the previous competition experiments and does
218 not allow us to calculate selection coefficients, we could qualitatively screen all
219 subcommunities for their selective effect on the evolved porin mutant by determining a
220 change in ratio from the 1:1 starting mixture to that after 24h of growth in presence of
221 different subcommunities (Fig. 2b). Most subcommunities enriched *K. pneumoniae ompK*^{evo}
222 over the wildtype in 24h of growth, but several subcommunities did no longer exhibit this
223 selective effect. The abundance of several genera showed a positive correlation with selection
224 of *K. pneumoniae ompK*^{evo} over the wildtype, such as *Sutterella, Parabacteroides* and
225 *Escherichia* (Extended Data Fig. 5). The latter was of particular interest, as certain conditions,
226 such as bile salts, resulted in sub-communities dominated by *E. coli,* while maintaining their
227 selective effect on *K. pneumoniae ompK*^{evo} (Fig. 2b). To test whether *E. coli* is sufficient to drive
228 the selection of *K. pneumoniae ompK*^{evo}, we isolated the resident *E. coli* s from MB003
229 (hereafter called *E. coli*^{MB003}) and showed that co-culturing it with the *K. pneumoniae*
230 competitors was enough for the *K. pneumoniae ompK*^{evo} to outcompete its susceptible
231 wildtype by about 2% (Extended Data Fig. 6). Although subcommunities depleted for *E. coli*
232 (such as after sparfloxacin or cefotetan treatment) were still selective for *K. pneumoniae*
233 *ompK*^{evo} (Fig. 2b), we show that *E. coli* is sufficient to drive part of this selection.

234

235 **High-order community interactions can modulate the selective advantage *E. coli* provides**
236 **for *K. pneumoniae ompK^{evo}***

237 *E. coli* is a common member of the human gut microbiome[38] and present in all fecal
238 microbiomes used in this study (Extended Data Fig. 7), raising the question why the selection
239 of *K. pneumoniae ompK^{evo}* occurred only in presence of MB003. To determine how specific
240 the observed effect was to the *E. coli* strain isolated from MB003, we performed competitions
241 of *K. pneumoniae ompK^{wt}* and *ompK^{evo}* in the presence of different *E. coli* strains. These came
242 from a diverse panel of 85 laboratory, environmental and pathogenic isolates[39], and included
243 the three *E. coli* strains isolated from MB001, MB002 and MB003 (Fig. 3a). The triple
244 competitions resulted into a wide range of selective coefficients for the *K. pneumoniae*
245 *ompK^{evo}*, ranging from no to approximately 4% fitness benefit. Notably in most cases in which
246 there was low/no selection for *K. pneumoniae ompK^{evo}*, this was linked to a poor ability of *E.*
247 *coli* to engraft in the community (Fig. 3a). This suggests that the selective effect exerted by *E.*
248 *coli^{MB003}* is a more general trait of *E. coli* rather than being specific to the MB003 strain.
249 Corroborating this, other *E. coli* strains isolated from fecal microbiomes used in this study also
250 exhibited strong selection (> 3% per cell per generation), even if their resident microbiome
251 did not select for the evolved porin mutant (Fig. 1g, 3a).

252

253 Given that the selective effect is generally provided by many *E. coli* strains, and that MB003 is
254 not enriched in *E. coli* compared to the other microbiomes (Extended Data Fig. 7), it implies
255 that other microbiota members, besides the residential *E. coli* strains, play a role in the
256 selective effect and significantly modulate its magnitude. To address such potential higher-
257 order interactions, we performed quadruple competition experiments including as a fourth
258 competitor one further bacterial species relevant to the human gut microbiota (Fig. 3b). In the
259 competition experiment, we inoculated *K. pneumoniae ompK^{evo}*, *K. pneumoniae* wildtype, *E.*
260 *coli^{MB003}* and the fourth competitor in equal proportions and followed their abundance over
261 three days of competition. We also labeled *E. coli^{MB003}* with a chromosomally encoded YFP
262 marker to be able to follow the abundance of all four strains in the competition. The presence
263 of a fourth competitor (untagged) modulated the selective advantage of *K. pneumoniae*
264 *ompK^{evo}* exerted by *E. coli* in different ways. For example, the presence of other enterobacteria
265 or *Prevotella copri* increased the selective advantage of *K. pneumoniae ompK^{evo}* in presence

266 of *E. coli*^{MB003} to 3 percent, while the presence of *Clostridium perfringens* strongly alleviated
267 the fitness advantage. Notably, these modulating effects align with compositional differences
268 observed in MB003, which exhibits lower abundance for *Clostridiales* and higher abundance
269 of *Prevotella* compared to the other fecal microbiomes (Fig. 2a). Collectively, our results
270 demonstrate that while *E. coli* is sufficient to provide a selective advantage of *K. pneumoniae*
271 *ompK*^{evo} over its ancestral susceptible wildtype, higher order interactions in the community
272 shape the magnitude and even direction of the selection. This is likely the reason we see the
273 selective advantage only in MB003, and not in other microbiomes.
274
275 **Microbiome MB003 selects for *glyR* mutations that lead to upregulation of an alternative**
276 **porin**
277 To elucidate the underlying molecular mechanism that allowed for the evolved porin-mutant
278 to benefit in presence of MB003, we whole-genome sequenced seven *K. pneumoniae ompK*^{evo}
279 clones. All strains had acquired a mutation in a LacI-type transcription factor hereafter termed
280 'glycoporin regulator' (*glyR*). The mutational spectrum spanned frameshifts and substitutions
281 causing premature stop codons, internal deletions and single amino acid substitutions namely
282 T60P, I54S and C248W (Fig. 4a). *glyR* is located upstream of three genes encoding a putative
283 permease, hydrolase and porin. This is a common organization of a carbohydrate catabolic
284 operon where the transcription factor regulates expression of the structural genes, which
285 facilitate sugar uptake through the outer- and inner- membranes, followed by its hydrolysis in
286 the cytoplasm. In line with this hypothesis, whole cell proteomes of all seven isolated *K.*
287 *pneumoniae ompK*^{evo} mutants exhibited consistently strong and specific upregulation of all
288 three proteins encoded in the structural genes (Fig. 4b and Extended Data Fig. 8).
289
290 To determine which of the structural genes are causing the fitness advantage of the *glyR*
291 mutant background when grown in presence of MB003, we constructed several knockout
292 variants. Removing the whole operon, the predicted transcription factor binding sites or all
293 three structural genes resulted in a complete loss of the fitness advantage phenotype,
294 confirming that indeed the structural genes upregulated in the *glyR* mutant background are
295 causative. Furthermore, knockouts of each of the individual structural genes revealed that the
296 porin alone was sufficient for the fitness advantage (Fig. 4c). The porin (hereafter termed
297 glycoporin, GlyP) is predicted to belong to the raffinose porin family RafY (Extended Data Fig.

298 9), which contains a larger pore size compared to OmpK35/36 and is involved in the uptake of
299 a range of carbohydrates including oligosaccharides[40,41].
300
301 **Carbohydrate competition drives the selective advantage of the *glyR* mutants**
302 There are several potential mechanisms of how an increased expression of GlyP would provide
303 a fitness advantage in a community context. Since porins are involved in nutrient uptake, it is
304 conceivable that the fitness benefit is based on an increased nutritional competence.
305 However, porins also play a role in the uptake of toxins, export of metabolic waste products
306 or as receptors of phage and conjugative plasmids[42-44]. As such, an outer membrane with
307 different porin composition could render *K. pneumoniae ompK*^{evo} able to use a new niche or
308 to be more resistant to toxic products or to negative interactions with other community
309 members. To define the underlying mode of action of the evolved mutants, we grew *E.*
310 *coli*^{MB003} until saturation (20h), sterile filtered its supernatant, and used the spent medium to
311 determine growth characteristics of each *K. pneumoniae* strain in monocultures. *K.*
312 *pneumoniae ompK*^{evo} grew significantly better than its parental strains and the wildtype in the
313 spent medium (Fig. 5a), demonstrating that the selective effect mediated by *E. coli* is contact
314 independent. Supplementing the spent medium with a good carbon source (0.2% glucose),
315 resulted in higher growth yields and similar growth characteristics of all three *K. pneumoniae*
316 strains (Fig. 5b), indicating that: a) the lack of carbon sources is growth-limiting for *K.*
317 *pneumoniae* in these conditions, and b) the selection advantage of *ompK*^{evo} is only visible in
318 poor nutrient conditions and hence most likely works via increased nutritional competence,
319 as growth inhibitory mechanisms like toxin uptake or phage susceptibility would have
320 manifested independently of the absence or presence of glucose.
321
322 MGAM is a rich medium designed to support the growth of a wide range of gut-derived
323 bacteria, and hence it contains a plethora of potential carbon sources that could create a
324 metabolic niche that selects for *K. pneumoniae ompK*^{evo}. To narrow down the spectrum of
325 potential candidate compounds, we performed thermal proteome profiling (TPP)[45,46]. Due to
326 the fact that enzyme-substrate interactions lead to thermal stabilization[47], TPP has the
327 potential to identify catabolic pathways that are thermally stabilized in *K. pneumoniae*
328 *ompK*^{evo}, but not in the *K. pneumoniae* wildtype, in the presence of the *E. coli*^{MB003} spent
329 medium. Indeed, by treating whole cell lysates of *K. pneumoniae* wildtype and *K. pneumoniae*

330 *ompK*^{evo} mutant with *E. coli*^{MB003} spent medium, we identified several proteins that were
331 thermally stabilized only in the *K. pneumoniae ompK*^{evo} lysate (Fig. 5c). In addition to GlyP
332 itself, which was higher expressed in the *ompK*^{evo} cells (Fig. 4b), two of the most strongly
333 stabilized proteins in spent-medium treated *K. pneumoniae ompK*^{evo} were DhaT and GlpK,
334 both of which are involved in glycerol catabolism. DhaT is the 1,3-propanediol dehydrogenase,
335 which converts 3-hydroxypropionaldehylde (generated from glycerol by a dehydratase) to 1,3-
336 propanediol, and GlpK is the glycerol kinase. The strong stabilization of both enzymes
337 suggested that glycerol, or glycerol-derivatives, were present in the spent media, and that
338 glycerol catabolic enzymes were active in *K. pneumoniae ompK*^{evo} but not in the wildtype.
339
340 To determine whether glycerol or glycerol derivatives were available in the spent medium, we
341 decided to measure the metabolites present in the *E. coli*^{MB003} spent medium before and after
342 growth of *K. pneumoniae ompK*^{evo}. We chose eight different *E. coli* strains that were selective
343 for *K. pneumoniae ompK*^{evo} as well as three *E. coli* strains that were not (Fig. 3a), and prepared
344 spent medium of each strain individually. By profiling the growth of *K. pneumoniae* wildtype,
345 *K. pneumoniae ompK*^{mut} and *K. pneumoniae ompK*^{evo} in these spent media, we could confirm
346 that the growth characteristics in the various spent media (Extended Data Fig. 10) were
347 consistent with the selective coefficients determined in the co-culture experiments (Fig. 3a).
348 *K. pneumoniae ompK*^{evo} showed a growth advantage in spent media prepared from 'selective'
349 *E. coli* strains, while it grew equally well to the wildtype in spent medium prepared from 'non-
350 selective' *E. coli* strains (Extended Data Fig. 10). We then subjected all spent media before and
351 after growth of *K. pneumoniae ompK*^{evo} to untargeted metabolomics to determine which
352 compounds were produced or consumed by *K. pneumoniae* (Fig. 5d). While we did not detect
353 free glycerol in the samples, we identified several glycerol-containing compounds that were
354 (i) present in mGAM, (ii) not consumed by *E. coli*, and (iii) consumed after growth of *K.*
355 *pneumoniae ompK*^{evo} (Fig. 5e and Extended Data Fig. 11). As such, Glyceryl-5-
356 hydroxydecanoate was significantly reduced in abundance in all spent-media prepared from
357 'selective' *E. coli* isolates. While also found in spent media derived from non-selective *E. coli*,
358 it was either consumed to a low degree (iAI16 and NT12033) or present at a lower levels (iAI16
359 NT12072) compared to spent media derived from 'selective' *E. coli*. Judging from the robust
360 growth of all *K. pneumoniae* strains in the spent media of non-selective *E. coli* strains

361 (Extended Data Fig. 10), it is likely that other better carbon sources are available to them, akin
362 to when glucose is present in the spent medium of *E. coli*^{MB003} (Fig. 5b).
363
364 To unambiguously show that selection of *K. pneumoniae ompK*^{evo} is due to an advantage to
365 catabolize glycerol, we performed competition experiments of *K. pneumoniae* wildtype vs
366 either *K. pneumoniae ompK*^{mut} or *ompK*^{evo} in minimal medium supplemented with glycerol or
367 glucose as the sole carbon sources. While *K. pneumoniae ompK*^{mut} grew similarly to the
368 wildtype in glycerol, the *K. pneumoniae ompK*^{evo} exhibited a significantly increased fitness of
369 around 4% per cell per generation compared to the wildtype. This fitness advantage was
370 specific to glycerol, as the evolved mutant grew similarly as the wildtype with glucose as the
371 sole carbon source (Fig. 5f). To determine if the selective advantage of *glyR* mutants is specific
372 for growth on glycerol, we tested a series of additional carbon sources for their impact on
373 fitness of *K. pneumoniae ompK*^{mut} and *K. pneumoniae ompK*^{evo} compared to the wildtype. In
374 stark contrast to growth on glycerol, we observed that other carbon sources, such as fructose,
375 lactose or maltose were disfavoring the *K. pneumoniae ompK*^{evo} with counterselection
376 coefficients reaching up to 9% per cell per generation.
377
378 In summary our results show, that treatment of *glyR* mutant lysates with *E. coli* spent medium
379 causes thermal stabilization of glycerol catabolic enzymes (indicating their metabolic activity),
380 that mGAM contains glycerol-derivatives that are consumed by *K. pneumoniae*, but not by *E.*
381 *coli*, and that the *glyR* mutant has a selective advantage when grown in presence of glycerol
382 as the sole carbon source. This suggests that specific microbiota composition(s) can create a
383 niche for consumption of glycerol derivatives. This drives the selection of mutations in *glyR*,
384 which lead to increase in GlyP expression in the *ompK35/36* mutant.
385
386 **_glyR_ mutations are under strong positive selection in clinical _K. pneumoniae_ populations**
387 We next exploited a large collection of publicly-available genomes of the globally-important
388 high-risk lineage, clonal complex (CC) 258, which includes ST258 and other closely-related STs.
389 Thereby we could assess the sequence variation and evolution within the *glyP* operon, and
390 determine if the selective pressures identified in our *in vitro* screen are clinically relevant. In
391 particular, we generated a mapping-based chromosomal alignment of 9214 high-quality
392 CC258 genomes and used an ancestral reconstruction approach that, for each chromosomal

393 base position, inferred the ancestral base state at all nodes across a recombination-free
394 phylogenetic tree. For each base position, we analyzed the occurrence and frequency of base
395 (state) changes across the phylogenetic tree, with a focus on the *glyP* operon. While the
396 structural genes within the operon showed only a few base changes with no more than 3 SNPs
397 occurring at any individual base position, we identified a single mutational hotspot (C->A) at
398 position 4,366,094 (with respect to the HS11286 reference genome), corresponding to the
399 T60P substitution in GlyR (Fig. 6a). We estimate that this substitution occurred independently
400 35 times across the CC258 phylogeny. Interestingly, we identified the same substitution in our
401 *in vitro* screening (Fig. 4a), confirming that the *in vitro* selection driven by MB003 in mGAM is
402 recapitulating selective pressures acting on clinical *K. pneumoniae* populations. Notably, we
403 also identified a distinct subclade in which *glyR* is entirely absent due to a deletion spanning
404 the gene (Fig. 6b, clade B). Consistent with this pattern, our *in vitro* screen also identified
405 premature stop codons and frameshift mutations in *glyR* (Fig. 4a).
406
407 Despite the *glyR* T60P mutation emerging frequently across the CC258 population, its sporadic
408 occurrence on terminal or near-terminal branches of the phylogenetic tree, and subsequent
409 presence in only 41/9214 (0.4%) of CC258 genomes, suggests that this mutation cannot
410 expand clonally (Fig. 6b). This is in contrast to what is expected for mutations that are under
411 long-term positive selection, which would expand within larger clades of the tree. This
412 absence of clusters is indicative, that *glyR* mutations are likely under strong positive selection
413 in some conditions, but then become disadvantageous and are quickly counter-selected when
414 conditions change. This is in line with our findings, that *K. pneumoniae ompK*^{evo} is only selected
415 in certain microbiomes (Fig. 1g), and that *K. pneumoniae ompK*^{evo} has no benefit, or even
416 strong fitness defects, when growing on other carbon sources than glycerol (Fig. 5f). Together,
417 these findings show that GlyP upregulation bestows a conditional selective advantage for *glyR*
418 mutations in *K. pneumoniae* in the presence of glycerol-containing niches, but these
419 mutations are an evolutionary dead-end when the available niche changes.
420

421 ## Discussion

422 Here, we determined the impact of diverse human gut microbiotas on the fitness of a
423 prevalent antibiotic resistance mutation in the ESKAPE pathogen *K. pneumoniae*. We

424 discovered that a specific microbiota drove the evolution of a high-fitness variant in the *K.*
425 *pneumoniae* resistant strain. The fitness benefit was caused by mutations in the
426 transcriptional regulator *glyR*, which resulted in the upregulation of an alternative porin, GlyP.
427 By using proteomic, metabolomic and phenotypic analyses we identified nutrient competition
428 for glycerol-containing compounds as the driving factor of the selection.
429
430 The general exclusion of intruding, usually pathogenic, species by the residential microbiota
431 is termed colonization resistance, and is an important property of a healthy microbiome.
432 Various studies have shown the benefit of resident/probiotic bacterial species in preventing
433 the invasion of pathogenic isolates[48-51]. Carbohydrate competition has been shown to play a
434 key role in colonization resistance against various pathogens, including, *E. coli*[50], *K.*
435 *pneumoniae*[49,52] and *S. enterica* serovar Typhimurium[48,49], where direct competition for
436 consumption of specific carbon sources such as galactitol or beta-glycosides can restrict
437 growth of pathogenic bacteria. Here we show that nutrients, and specifically glycerol
438 catabolism, drives the evolution and enrichment of an antibiotic resistant *K. pneumoniae*
439 porin-mutant. Although we showed that *E. coli* was at least partially responsible for the
440 creation of this selective niche, higher-order interactions with other community members
441 augmented or removed the selection. For example, *Clostridium perfringens* removed the
442 selective niche. Interestingly, *E. coli* is unable to utilize glycerol as the sole carbon source under
443 strictly anaerobic conditions, while *K. pneumoniae* and members of the *Clostridiales* family
444 can[53-55]. Thus, we propose a model where *E. coli* is exerting its selective effect for the high-
445 fitness K. *pneumoniae* porin-mutant not by direct carbohydrate competition, but rather by
446 creating a niche by removing other, more favorable carbon sources.
447
448 Furthermore, we show that the selection for the high-fitness *K. pneumoniae* porin mutant is
449 context-dependent, as the *glyR* mutations are detrimental in other conditions. Clinical *K.*
450 *pneumoniae* isolates seem to be subjected to similar selective pressures, as shown by the
451 recurrent emergence of the *glyR* T60P mutation among clinical isolates. At the same time, and
452 in line with the results we presented here, the selective pressures are highly conditional,
453 limiting the clonal expansion *of K. pneumoniae* carrying *glyR* mutations. It is conceivable that
454 these mutations occur in isolated patients with favorable microbiome composition and dietary
455 habits, but are not competitive when the environment changes (diet or microbiome)

restricting their expansion and transmission. Identifying and understanding selective pressures against (high-fitness) antibiotic-resistant pathogens could enable us to drive off antibiotic resistant strains by dietary modulation.

Strategies for decolonization of pathogens from microbiomes are currently being discussed and actively researched[56]. However counter-selection of an opportunistic pathogen from a 'healthy' microbiome opens a niche that could be covered by other invading pathogens. In contrast, finding conditions that specifically counter-select antibiotic-resistant variants of native opportunistic pathogens of the human gut microbiome (e.g. in *K. pneumoniae* or *E. coli*) would avoid this opening of the niche for new invaders. Instead this would allow the antibiotic susceptible strains of the same species to replace their resistant counterparts, and make treatment easier would the opportunistic pathogen lead to infection. Our study lays out a roadmap for how to identify potential probiotic bacteria and/or dietary compounds restricting growth of antibiotic-resistant bacteria that could subsequently be used to drive out antibiotic resistant pathogens from healthy gut microbiomes, decreasing the risk of acquiring hard-to-treat infections in the future.

472 **Materials and Methods**

473 Isolation of fecal microbiome samples

474 Fresh fecal samples from nine healthy donors were collected and transferred directly into an
475 anaerobic chamber. Samples were mixed at a 1:1 ratio (w/v) with PBS containing 40% glycerol
476 and 0.5 g/L cysteine, homogenized, and aliquoted into cryovials for preservation. At the time
477 of sample collection, one aliquot was inoculated into 50 ml of mGAM medium, serially diluted,
478 and incubated anaerobically at 37 ºC for 24 h. Following incubation, 800 µl of the diluted
479 cultures was combined with 200 µl of 50% glycerol and preserved at −80 ºC. The collection of
480 human stool samples and all related experiments were approved by the EMBL Bioethics
481 Internal Advisory Committee. Informed consent was obtained from all donors (EMBL
482 BIAC2015-009). The synthetic community was assembled as previously described[35,57]. In brief,
483 monocultures of each species were grown overnight in mGAM broth anaerobically at 37 ºC,
484 adjusted to OD_{600} = 0.01, mixed at equimolar ratios and cryopreserved in 15% glycerol. For
485 community experiments, the frozen community was reconstituted in fresh mGAM by a 1:100
486 dilution and grown for 24 hours in mGAM broth anaerobically at 37 ºC.

487

488 DNA extraction

489 Genomic DNA was isolated in 96-well deep-well plates. Cells were washed in PBS, and pellets
490 were resuspended in cell suspension solution (281 µl) from the GNOME DNA isolation kit (MP
491 Biomedicals). Resuspended cells were enzymatically digested with lysozyme (25 µl; 400,000 U
492 ml−1, Sigma) at 37 ºC for 1h. Lysis was further enhanced by three freeze-thaw cycles in liquid
493 nitrogen, followed by the addition of the kit's lysis solution (15.2 µl) and RNA mix (20 µl). A
494 final lysis step was conducted using glass beads (Glasperlen, Edmund Bühler) with bead-
495 beating (5 min x 2 at 30 Hz) in a Tissue Lyzer II (Qiagen). Lysates were then incubated at 37 ºC
496 with shaking for 30 min, followed by protease treatment (12.8 µl; GNOMETM kit) at 55 ºC for
497 2h. Cell debris was removed by centrifugation (3200 g, 5 min) and 200 µl of the supernatant
498 was mixed with 100 µl of TENP buffer (50 mM Tris-HCl pH 8, 20 mM EDTA, 100 mM NaCl, 1%
499 polyvinylpolypyrrolidone). The mixture was incubated for 10 min at 4 ºC with 75 µl of salt out
500 solution (GNOME kit), followed by 10 min centrifugation at 3200 g. 200 µl of supernatant was
501 transferred to a fresh plate, mixed with 500 µl of ice-cold ethanol and 70 µl of 3 M NaOAc pH
502 5.2 were added, and kept at −30 ºC overnight to precipitate DNA. The next day, DNA was

503 pelleted (3200 g, 45 min, 4 ºC), washed with 70% ethanol, air-dried, and rehydrated in
504 molecular-grade water at 4 ºC.
505
506 16S sequencing
507 For sequencing, 16S rRNA gene libraries were prepared using a two-step PCR approach with
508 Phire Hot Start II DNA Polymerase (Thermo Fisher Scientific). The V4 region was first amplified,
509 and a second PCR was carried out with indexed primers containing Illumina adaptors. Libraries
510 were sequenced using paired-end chemistry (2 x 250 bp) on a MiSeq platform.
511
512 Raw sequencing reads from WGS and 16S data were processed using bbduk (v38.91). For WGS
513 data, reads underwent several preprocessing steps to remove low-quality sequences: Low-
514 quality bases were trimmed from both ends (qtrim = rl, trimq = 3), followed by the removal of
515 entire reads falling below a quality threshold (maq = 25). Adapter sequences were then
516 removed (ktrim = r, k = 23, mink = 11, hdist = 1, tpe = true, tbo = true) and reads shorter than
517 75 base pairs were discarded. For 16S data, reads underwent low-quality base trimming (qtrim
518 = rl, trimq = 10), followed by targeted removal of 5' amplicon primers from R1 and any
519 potential reverse complement primers from R2 (ktrim = l, k = 9, mink = 1, hdist = 1, restrictleft
520 = 50, maq = 20). Similarly, 3' primers were removed from R2, along with any potential reverse
521 complement sequences from R1 (ktrim = r, k = 9, mink = 1, hdist = 1, restrictright = 50, maq =
522 20). Finally, reads shorter than 75 base pairs were discarded.
523
524 Metagenomic sequencing
525 Microbial DNA was extracted from collected stool samples using Qiagen AllPrep PowerFecal
526 Pro DNA/RNA Kit (Qiagen, Hilden, Germany) following the manufacturer's protocol.
527 Metagenomic sequencing libraries were prepared using the NEBNext Ultra II DNA Library Prep
528 kit (New England Biolabs, MA, USA) with a targeted insert size of 350-400bp and Dual Index
529 multiplex oligos. Libraries were prepared using a liquid automated system (Beckman Coulter
530 i7 Series) and sequenced on an Illumina HiSeq 4000 platform (Illumina, San Diego, CA, USA)
531 with 2x150bp paired-end reads.
532
533 Taxonomic profiling

534 For profiling of 16S data, we used IDTAXA84 from the DECIPHER package (v3.0.0)[58] with
535 parameters strand = both and threshold = 40 and the GTDB r207 (modified) training set. WGS
536 data were profiled using mOTUs (v3.1)[59] with default settings.
537
538 Community competition experiments
539 All competition experiments were performed at 37 ºC in an anaerobic chamber (Coy
540 laboratory Products; 2% H2, 12% CO2, 86% N2) in modified Gifu anaerobic medium (mGAM)
541 broth (HyServe, produced by Nissui Pharmaceuticals). For competitions in complex
542 communities, aliquots of the cryopreserved fecal microbiomes were thawed under anaerobic
543 conditions and 50µl were diluted in 5ml MGAM and grown overnight. The subsequent day,
544 the cultures were diluted in fresh mGAM broth to a final OD_{600} of 0.01. Overnight cultures of
545 the fluorescently labeled *K. pneumoniae* competitors were mixed at equimolar ratios and
546 added to the OD_{600}-adjusted communities at a final OD600 of 0.001, leaving a 10-fold excess
547 of community members compared to *K. pneumoniae* competitors. Each day, the competition
548 cultures were diluted 1:1000 in fresh mGAM broth to a final volume of 1ml. Each competition
549 experiment was conducted in two configurations: one in which strain A was tagged with GFP
550 and strain B with RFP, and another in which the fluorescent markers were reversed. Each
551 configuration was tested with a minimum of five biological replicates. Additionally, we
552 competed two independently constructed sets of the *K. pneumoniae* wild type carrying either
553 GFP or RFP with 10 biological replicates under each condition (microbiome) to determine the
554 fitness effect imposed by marker expression. The selection coefficients determined for the *K.*
555 *pneumoniae* wild type tagged with GFP or RFP were subsequently subtracted from selection
556 coefficients of GFP or RFP positive strains accordingly.
557
558 Competition in defined communities (triple competitions in presence of *E. coli* or quadruple
559 competition in the presence of an additional fourth competitor) were performed in a similar
560 fashion. Each competitor was grown overnight in mGAM and mixed at equimolar ratios to a
561 starting OD_{600} of 0.01. Competition experiments with defined carbon sources were performed
562 in M9 minimal medium (0.1 mM $CaCl_2$, 1mM $MgSO_4$, 1x M9 Salts (Sigma Aldrich))
563 supplemented with the carbon source of interest at a final concentration of 0.2%.
564

565 To determine the ratios of GFP^+, RFP^+ or GFP^-/RFP^- cells, 50µl aliquots were removed from
566 each passage, washed twice with PBS and samples were resuspended in 50µl PBS. The
567 samples were incubated for 2h at room temperature under aerobiosis to allow maturation of
568 the fluorescent proteins. After two hours cells were fixed by adding an equal amount of 4%
569 Paraformaldehyde and incubating for 10 minutes. After fixation, cells were washed once with
570 PBS and taken up in 150µl final volume PBS. Samples were subjected to flow cytometry to
571 determine the ratio of the RFP^+ and GFP^+ competitors, as well as the untagged microbiome
572 using the Aurora spectral analyzer (Cytek Biosciences). In rare cases, individual wells were
573 excluded from analyses where fluorescent populations could not be clearly distinguished from
574 non-fluorescent background events, likely due to incomplete resuspension before aeration
575 causing a failure in fluorescent protein maturation.
576
577 Whole genome sequencing
578 To isolate the endpoint *K. penumoniae* strains, competition cultures were streaked out on LB
579 (5 g yeast extract, 10 g Tryptone, 10 g NaCl L^{-1}) Agar plates containing 50 mg/L Carbenicillin
580 and incubated aerobically at 37°C overnight, which specifically selects for the growth of K.
581 pneumoniae. GFP or RFP tagged colonies were differentiated using a Flu-O-Blu
582 transilluminator (Biozym). Colonies of interest were purified by streaking on LB agar plates
583 and incubating at 37 °C overnight. The isolates were then grown overnight in LB broth and
584 cryopreserved using 15% glycerol. 1 ml of each culture was used to extract genomic DNA
585 using the MasterPure DNA purification kit according to the manufacturer's recommendations
586 (Epicentre). All samples were subjected to whole-genome sequencing using a MiSeq system
587 (Illumina, USA). The paired-end sequence reads were trimmed and mapped using CLC
588 Genomics Workbench (CLC Bio, Denmark) using standard parameters. Subsequently,
589 inversion, deletions, structural variants, and single nucleotide polymorphisms were
590 determined using standard parameters.
591
592
593 Subcommunity enrichment
594 Forty-eight growth conditions were established (Supplementary Table X). Drug compounds,
595 except rifaximin which was freshly prepared, were dissolved as 100x stock solutions in
596 ethanol, DMSO, or water, as appropriate, and stored at −20 °C in 96-well drug plates. Rich and

597 selective media were freshly prepared and stored at room temperature. Twenty-four hours
598 prior to inoculation, all materials and reagents were transferred into an anaerobic chamber
599 (Coy Laboratories). On the day of inoculation, drug/medium plates were assembled under
600 anaerobic conditions by mixing 100 µl of medium with the compounds in the drug plate,
601 followed by transfer of 115 µl of the resulting drug–medium mixture back into the deep-well
602 plate. For medium-no drug conditions, 1,485 µl of medium was added to the corresponding
603 well.
604
605 Cryopreserved stool from donor MB003 (700 µl aliquot, prepared as described above) was
606 diluted 1:100 in PBS, and 15 µl of this suspension was inoculated into each of the 48 wells of
607 a 96-well deep-well plate containing 1,485 µl of medium (~5×10^7 CFU ml^{-1} final). Cultures
608 were incubated anaerobically at 37 °C for 24 h, then sequentially passaged for three additional
609 days by 1:50 dilution into fresh drug/medium plates. Growth was monitored daily by
610 transferring 100 µl of culture into shallow 96-well plates and measuring optical density at 578
611 nm every hour for 24 h. On day 5, 500 µl of each culture was mixed with glycerol for long-term
612 storage, and the remaining culture (~1 ml) was collected for DNA extraction.
613
614 *E. coli* was isolated from the bile-salt-treated subcommunity by plating on LB agar plates and
615 incubating at 37°C under aerobic conditions overnight. Colonies were purified and species was
616 determined by 16S sequencing. After confirmation, that the isolated *E. coli* strain is selective
617 for *K. pneumoniae ompK*^{evo}, whole genome sequencing of the strain was performed as
618 described previously.
619
620 Construction of knockout mutants
621 Gene knockouts were constructed using the lambda red recombineering system encoded on
622 the synthetic vector pSIM5-tet [60,61]. Overnight cultures of the strain of interest were diluted
623 1:100 fold in 50 ml LB broth at 37°C with constant shaking to a final OD600 of 0.2. Cells were
624 harvested and washed three times with ice-cold 10% glycerol and taken up in a final volume
625 of 100µl. 40µl cells were mixed with 50 ng of pSIM5 tet and transferred to an electroporation
626 cuvette (1-mm gap). Electroporation was performed using a Gene Pulser (Bio-Rad) at 1.9kV,
627 400 Ohm and 25µF. After electroporation, cells were recovered in 1ml SOC (2% trypton, 0.5%

628 yeast extract, 10 mM NaCl, 2.5 mM KCl, 10 mM $MgCl_2$, 10 mM $MgSO_4$ and 20 mM Glucose)
629 for 2 hours, plated on LB Agar plates containing 10 mg/L tetracycline and incubated at 30°C.
630
631 To prepare electrocompetent cells, pSIM5-tet carrying strains were grown overnight in LB
632 broth supplemented with 10 mg/L tetracycline at 30°C, diluted 1:100 in 50 ml LB broth
633 supplemented with 10 mg/L tetracycline and incubated at 30° until they reached OD600 =
634 0.02. Cultures were moved to a 42°C water-bath to induce expression of the lambda red
635 system for 15 minutes. Afterwards, the cultures were placed on ice for 10 minutes and washed
636 3 times with ice-cold 10% glycerol. The cells were resuspended in 200µl 10% glycerol final
637 volume, and 40µl were mixed with a 200ng purified PCR product of a gene construct
638 containing *amilCP* (blue chromoprotein), *cat* (chloramphenicol resistance) and *sacB* (sucrose
639 sensitivity) with homologous overhangs up- and downstream of the gene of interest.
640 Electroporation and cell recovery were performed as described above. Successful
641 transformants were selected on LB agar plates supplemented with 15 mg/L chloramphenicol
642 at 30°C. Transformants were restreaked on LB agar plates supplemented with 10 mg/L
643 tetracycline at 30°C to ensure maintenance of pSIM5-tet. The strains were then subjected to
644 a second round of transformation as described above. Here, instead of a PCR product, single-
645 stranded DNA was electroporated composed only of the up- and down-stream homologous
646 overhangs, to replace the amilCP-cat-sacB cassette leaving a scarless knockout. Recovery of
647 transformants was performed in 5 ml SOC overnight to ensure dilution of the SacB protein in
648 cells, and successful transformants were selected on salt-free LB agar plates supplemented
649 with 5% sucrose. Loss AmilCP, and therewith loss of the blue color, was an additional
650 verification, that the complete amilCP-cat-sacB cassette was removed, and sucrose sensitivity
651 was not only lost due to a loss-of-function mutation in *sacB*. All final constructs were
652 confirmed by Sanger sequencing.
653
654 <u>Growth characterization in spent medium</u>
655 To prepare spent medium an overnight culture of the E. coli strain of interest was diluted
656 1:1000 in 20 ml mGAM under anaerobic conditions. The culture was grown for 20h, and cells
657 were pelleted by centrifugation for 10 minutes at 4000 rpm. The supernatant was transferred
658 and subjected to a second round of centrifugation. The supernatant of this second round was
659 sterile filtered using a filter with a 0.22µm pore size. The filtered supernatant was brought

660 back to anaerobic conditions and used as 'spent medium broth' for growth characterization
661 of the *K. pneumoniae* isolates. For this, overnight cultures of K. pneumoniae in mGAM were
662 diluted 1:2000 in spent medium. Growth rate was determined in 96-well plates sealed with
663 breathable membranes and OD600 was determined in 20-minute intervals over 24hours using
664 a Filtermax F5 multimode plate reader (Molecular Devices). The first timepoint was used for
665 background subtraction. All growth rate determinations were performed in triplicate.
666
667
668 Estimating the occurrence and frequency of SNPs across the *glyP* operon among *K.*
669 *pneumoniae* CC258 genomes
670 We generated a large collection of CC258 genomes from publicly-available genomes available
671 in Pathogenwatch (https://pathogen.watch)[62]. Raw sequence reads associated with these
672 genomes were downloaded from the European Nucleotide Archive (ENA) using available
673 accession numbers. Reads were mapped to the ST11 reference genome, HS11286 (accession
674 CP003200) using a workflow (https://gitlab.com/cgps/ghru/pipelines/snp_phylogeny)
675 (version 1.2.2) incorporating BWA-MEM (Li, 2013), SAMtools and BCFtools[63] and a pseudo-
676 genome alignment was generated. Genomes were excluded from downstream analyses if they
677 had < 20x average mapping depth or ≥ 25% missing sites in the pseudo-genome alignment.
678 Gubbins v3.2.1[64] was used to remove recombined regions from the alignment and generate a
679 maximum likelihood tree with RAxML-NG[65]. For each base position within the pseudo-
680 genome alignment, a maximum parsimony method was used to perform ancestral
681 reconstruction across the tree (https://github.com/sanger-pathogens/bact-gen-
682 scripts/blob/master/reconstruct_snps_on_tree.py). The number of state changes inferred to
683 have occurred across the tree at each base position was calculated and the types of SNPs
684 recorded.
685
686
687 Genotypic characterization of genome assemblies
688 Genome assemblies from the above-described CC258 collection were additionally
689 characterized. Kleborate v2.3.0 was used to identify virulence and resistance genes including
690 alterations within the *ompK35* and *ompK36* porin genes[66]. These included truncations of both
691 genes, and loop 3 insertions (glycine-aspartate (GD) or threonine-aspartate (TD)) within

692 *ompK36*. The *lacI* type transcription factor was identified among the assemblies using BLASTn
693 v2.14.1[67] with the full-length gene from ATCC43816 (accession CP009208) as the query
694 sequence. We required a single hit in each assembly that matched ≥25% of the query length
695 and contained a start codon to unambiguously identify the gene. Nucleotide sequences were
696 translated to protein sequences using Seaview v5.0.5[68]. Protein sequences were predicted to
697 be intact if they possessed at least 90% of the query length. Metadata and genotypic data
698 were visualised with the phylogenetic trees using Microreact v273[69].
699
700 The Artemis Comparison Tool (ACT) v18.1.0[70] was used to compare the ST11 genome,
701 HS11286, with a representative genome assembly from the clade of 306 CC258 isolates with
702 an absent lacI type TF gene (SRR12509433). Prior to the comparison, the contigs from
703 SRR12509433 were aligned and reordered against the HS11286 complete genome using
704 Abacas v1.3.1[71].
705
706 Metabolite extraction
707 LC-MS grade solvents were purchased from Fisher Scientific, and all other chemicals from
708 Sigma Aldrich, unless otherwise specified. For metabolite extraction, 20 µL of the bacterial
709 supernatants were transferred in a 96-well plate with 105 µL of ACN:MeOH solvent mixture
710 in a 1:1 ratio supplemented with an internal standard mixture. The internal standard mixture
711 contained sulfamethoxazole, caffeine, ipriflavone, and warfarin, each at 80 nM final
712 concentration. Following, the samples were chilled at -20°C for 1 h to allow proteins to
713 precipitate, then centrifuged at 4500 rpm for 15 min at 4 °C. The remaining supernatant was
714 finally aliquoted in 96-well microtiter plates, diluted with water (1:1), and an additional
715 centrifugation step at 4500 rpm for 15 mins and 4 °C.
716
717
718 LCMS analysis
719 LC-MS analysis was performed using reverse-phase chromatography in negative ionization
720 mode. Chromatographic separation was performed using an InfinityLab Poroshell 120 HILIC-Z
721 column (2.1 x 150 mm, 2.7-micron pore size) in an Agilent 1200 Infinity UHPLC system and
722 mobile phases A: H_2O + 5mM Ammonium formate + 0.1% formic acid and B: acetonitrile +
723 5mM Ammonium formate + 0.1% formic acid. The column compartment was kept at 25°C. 5

724 µL of the sample was injected at 98% B and 0.250 mL/min flow followed by: 98% B until minute
725 3, a gradient to 70% B until minute 11, a gradient to 60% B until minute 12, a gradient to 5%
726 B to minute 16, remaining at 5% until minute 18 before re-equilibration to 98% until minute
727 20. Flow remained at 0.250 mL/min.
728
729 The qTOF (Agilent 6550) was operated in positive scanning mode (50 – 1500 *m/z*) and
730 electrospray ionization (ESI) with the following source parameters: VCap: 3000 V, nozzle
731 voltage: 0 V, gas temp: 225 °C; drying gas 11 L/min; nebulizer: 40 psig; sheath gas temp 225°C;
732 sheath gas flow 10 L/min; fragmentor 300V and Octopole RF Vpp 450V. Online mass
733 calibration was performed using a second ionization source and a constant flow of reference
734 solution (121.0508 and 922.0097 *m/z*). Tandem mass spectrometry analysis (LC-MS/MS) was
735 performed for all significant metabolites using the chromatographic separation and source
736 parameters described above and the targeted-MS/MS mode of the instrument with a
737 preferred inclusion list for parent ion with 20 ppm tolerance, Iso width set to 'narrow width',
738 and collision energy set to either 10, 20, or 40 eV.
739
740 Data Extraction and Statistical Analysis
741 To reduce data complexity for downstream analysis, mass spectrometry data were centroided
742 and converted from the proprietary format (.d) to the m/z extensible markup language format
743 (.cef) using the peak picking algorithm of Agilent DAReprocessor at the following parameters:
744 minimum peaks height >= 5.000 counts; all ion species; only select common organic
745 compounds (no halogens); isotoping grouping with limit assigned charge states to a range of
746 1; compound filters based on Quality Score > 70. The .cef converted data represents each peak
747 in the mass-to-charge (*m/z*) dimension as a single, discrete peak in the mass spectrum,
748 reducing data size and the grouping of adducts for every molecular feature.
749
750 Following, the table of putative metabolic features, along with their relative intensities, was
751 then aligned with Agilent Mass Profiler Professional - MPP (version 15.1). In brief, feature
752 alignment allowed mass tolerances of 0.003 AMU or 20 ppm and retention time tolerance of
753 0.3 min or 3%; minimum absolute abundance 10.000 counts; minimum number of ions 3;
754 multiple charge states forbidden. The final feature table was also filtered to retain only
755 features that appear in 75% of replicates of at least one condition and submitted to MS1

756 feature annotation against the Metabolite and Tandem MS Database (METLIN) (v1233)[72] was
757 performed by Agilent MPP. Human Metabolome Database (HMDB) accession numbers were
758 also derived from METLIN, and compound classes were assigned based on the latest HMDB
759 release (v5.0)[73].
760
761 The resulting feature quantification table was processed in R (v4.4.1) using RStudio/2024.09.1,
762 applying an adapted protocol for blank removal, imputation, quantile normalization, and log-
763 transformation[74]. In brief, features with specific blank-to-sample ratios and samples with
764 abnormally low mean intensities were flagged as poor-quality and removed from analysis. The
765 remaining data were imputed to address missing values, in which a limit of detection (LOD)
766 threshold was established based on the minimum non-zero intensity in the data. Values below
767 this threshold were imputed to the LOD cutoff. Intensities were then quantile-normalized
768 using the normalize.quantiles function from the preprocessCore package (v1.64.0)[75] and
769 subsequently $\log_2$ transformed with a pseudo-count (half of the minimum positive value) to
770 stabilize variance was applied. For multivariate analysis such as PCA, data were also z-scored
771 (mean-centering and unit-variance scaling).
772
773 Multivariate and statistical analyses were performed in R 4.4.1 using RStudio/2023.06.1. First,
774 the prcomp function was used for Principal Component Analysis (PCA) for data visualization,
775 detection of sample outliers, and overall sample similarity. Volcano plots were done to
776 statistically compare spent media before and after Kpn inoculation. The significance of a
777 molecular feature was based on the intensity differences, in which the p-values were assessed
778 by t-test (t.test function in R). The p-values were FDR-corrected for multiple hypotheses
779 testing using the Benjamini-Hochberg procedure (p.adjust function in R with 'fdr' parameter).
780 Significant metabolites were selected when their intensity had a fold change > 0.5 and a
781 corrected p-value < 0.05. Finally, the area under the curve from significant features was
782 integrated using the MassHunter Quantitative Analysis Software (Agilent, version 7.0) based
783 on the accurate high-resolution mass and RT of the reference analytes with the following
784 parameters: signal threshold of 30,000; mass tolerances of 0.003 amu or 20 ppm; retention
785 time tolerance of 0.5 min. All metabolites annotated in this manuscript were assigned a Level
786 1 annotation according to the Metabolomics Standards Initiative (MSI) classification system.
787 This includes a match in retention time using the same chromatographic system, accurate

788 mass, and MS/MS fragmentation pattern, ensuring unequivocal identification of the
789 compounds.
790
791 Proteomics
792 For the differential abundance proteomics, cultures were grown anaerobically at °C to mid log
793 phase (OD600 = 0.5), washed once with PBS and snap frozen. Pellets were resuspended in 2%
794 SDS and incubated at 99 °C for 5 min.
795
796 TPP was performed as previously described[46,76]. In brief, *K. pneumoniae ompK*^{evo} cultures were
797 grown anaerobically at 37 °C overnight. Cells were then washed twice with anaerobic PBS,
798 resuspended in lysis buffer (50 ug/ml lysozyme, 1mM MgCl2, cOmplete protease inhibitors,
799 0.25 U/ul benzonase in PBS) and lysed with 5 freeze-thaw cycles. Crude lysates (protein
800 concentrations normalized to 10 ug/ul) were treated with filter-sterilized spent medium
801 prepared from various *E. coli* strains as described previously for 10 min at RT. Aliquots of
802 treated lysates were then incubated in 10 different temperatures for 3 min, followed by 3 min
803 at RT and 5min on ice. NP-40 was added to a final concentration of 0.8%, aggregates were
804 removed by filtration and soluble proteins were prepared for mass spec.
805
806 Proteins were prepared and digested as previously described[47,77]. Eluted peptides were
807 labelled with TMT16plex, for the differential abundance proteomics, and TMT18plex, for the
808 TPP experiment. Samples were then pooled (all samples of each two adjacent temperatures
809 for the TPP experiment) and pre-fractionated into 6 fractions under high pH conditions.
810 Samples were then analyzed with liquid chromatography coupled to tandem mass
811 spectrometry, as previously described[46].
812
813 For the differential abundance proteomics, MS data were processed as previously described[47].
814 Briefly, raw MS files were processed with isobarQuant[78] and the identification of peptide and
815 protein was performed with Mascot 1.0 (Matrix Science) against a FASTA database of
816 translated ORFs annotated in CP009208 modified to include known contaminants and the
817 reversed protein sequences. For the TPP experiment, raw files were converted to mzML
818 format using MSConvert from ProteoWizard, using peak picking, 64-bit encoding and zlib
819 compression, and filtering for the 1000 most intense peaks. Files were then searched using

820 MSFragger (v4.0)[79] in FragPipe (21.1) against a FASTA database of translated ORFs annotated
821 in CP009208 containing common contaminants and reversed sequences.
822 Data analysis was performed using R. Proteins with at least one uniquely identified peptide
823 were kept for the analysis. For the differential abundance proteomics, protein intensities
824 across all strains were normalized using variance stabilization normalization[80] and limma was
825 used to assess the differential expression of proteins. For the TPP experiment, protein
826 intensities across all conditions within each temperature were normalized as above and the
827 abundance and thermal stability scores were calculated as previously described [47,81]. To assess
828 the significance of abundance and thermal stability scores, limma was used [82].
829
830 **Supplementary material**
831 Extended Data Fig. 1 - Abundance of *K. pneumoniae* wildtype in different microbiomes over
832 the course of the competition experiment.
833 Extended Data Fig. 2 – Change in ratios over time of *K. pneumoniae* competitors in presence
834 and absence of various communities.
835 Extended Data Fig. 3 – Fit measures of selection coefficients
836 Extended Data Fig. 4 – Selection coefficient of *K. pneumoniae ompK*^{evo} in different
837 microbiomes.
838 Extended Data Fig. 5 – MB003 subcommunity selection of *K. pneumoniae ompK*^{evo} over *K.*
839 *pneumoniae*.
840 Extended Data Fig. 6 – Ratio of *K. pneumoniae ompK*^{evo} over the wildtype in presence of *E.*
841 *coli*^{MB003} over 40 generations of growth.
842 Extended Data Fig. 7 – Abundance of *E. coli* in native stool samples from MB001-MB010.
843 Extended Data Fig. 8 – Protein abundance changes in *K. pneumoniae ompK*^{evo} versus *K.*
844 *pneumoniae* wildtype.
845 Extended Data Fig. 9 – Structural prediction and comparisons for GlyP.
846 Extended Data Fig. 10 – Growth rates of *K. pneumoniae wildtype, ompK*^{mut} *and ompK*^{evo} in
847 various *E. coli*-spent media.
848 Extended Data Fig. 11 – Abundance of glycerol-containing metabolites in *E. coli*-spent media
849 in the presence or absence of *K. pneumoniae*.
850

Extended Data Table 1 – Whole proteome abundance changes in the *K. pneumoniae ompK*^{evo} clones versus the wild type

Extended Data Table 2 – Whole proteome thermal stability changes Whole proteome abundance changes in the *K. pneumoniae ompK*^{evo} clones versus the wild type in presence of *E. coli*^{MB003} spent medium

Data availability

Sequencing data of the *K. pneumoniae* isolates has been deposited in the European Nucleotide Archive (ENA) at EMBL-EBI under accession number PRJEB110171. *K. pneumoniae* CC258 genomes used in the ancestral reconstruction analysis are publicly-available with accessions included in the Microreact project: https://microreact.org/project/kp-cc258. The mass spectrometry proteomics data have been deposited to the ProteomeXchange Consortium via the PRIDE partner repository with the dataset identifier PXD075097. The metabolomics data is available in the MetaboLights database (https://www.ebi.ac.uk/metabolights/) under accession number MTBLS7388.

Acknowledgements

We thank A. Mateus for assistance with proteomic analyses, D. Hazenbrink and C. G. P. Voogdt for assistance with subcommunity enrichments of fecal microbiomes, Maria I. Keller for DNA extraction of fecal microbiome samples and S. Giri for valuable discussions throughout the project. We also thank the EMBL core facilities for Genomics, Metabolomics, Proteomics, Flow Cytometry and Microbial Automation & Culturomics for their extended support throughout the project.

Author contribution

M.K. and A.T. acquired funding and conceptualized the study. M.K., S.G-S., L.M, D.P., V.C. and D.M.S. performed the experiments. S.D., J.L.C.W. and N.K. performed the computational analysis. G.F., M.Z., M.M. and A.T. supervised this study. M.K., L.M., D.P., S.D. and N.K. visualized the data and generated the figures. M.K. and A.T. wrote the original draft of the

manuscript. All authors discussed the results and reviewed and edited the final version of the manuscript.

Funding.

This work was supported by a postdoctoral research grant of the Swedish research council (2019-00666) to M.K., the ERC consolidator grant uCARE (ID 819454), EMBL core funding and an Infection Biology Transversal Theme Synergy Grant to A.T.

Conflict of interest

The authors declare no conflict of interest.

References

1 Teillant, A., Gandra, S., Barter, D., Morgan, D. J. & Laxminarayan, R. Potential burden of antibiotic resistance on surgery and cancer chemotherapy antibiotic prophylaxis in the USA: a literature review and modelling study. *Lancet Infect Dis* **15**, 1429-1437 (2015). https://doi.org:10.1016/S1473-3099(15)00270-4

2 Antimicrobial Resistance, C. Global burden of bacterial antimicrobial resistance in 2019: a systematic analysis. *Lancet* **399**, 629-655 (2022). https://doi.org:10.1016/S0140-6736(21)02724-0

3 Collaborators, G. B. D. A. R. Global burden of bacterial antimicrobial resistance 1990-2021: a systematic analysis with forecasts to 2050. *Lancet* **404**, 1199-1226 (2024). https://doi.org:10.1016/S0140-6736(24)01867-1

4 Farha, M. A., Tu, M. M. & Brown, E. D. Important challenges to finding new leads for new antibiotics. *Curr Opin Microbiol* **83**, 102562 (2025). https://doi.org:10.1016/j.mib.2024.102562

5 Hutchings, M. I., Truman, A. W. & Wilkinson, B. Antibiotics: past, present and future. *Curr Opin Microbiol* **51**, 72-80 (2019). https://doi.org:10.1016/j.mib.2019.10.008

6 Ross, J. D. C. *et al.* Oral gepotidacin for the treatment of uncomplicated urogenital gonorrhoea (EAGLE-1): a phase 3 randomised, open-label, non-inferiority, multicentre study. *Lancet* **405**, 1608-1620 (2025). https://doi.org:10.1016/S0140-6736(25)00628-2

7 Imai, Y. *et al.* A new antibiotic selectively kills Gram-negative pathogens. *Nature* **576**, 459-464 (2019). https://doi.org:10.1038/s41586-019-1791-1

8 Pahil, K. S. *et al.* Author Correction: A new antibiotic traps lipopolysaccharide in its intermembrane transporter. *Nature* **631**, E18 (2024). https://doi.org:10.1038/s41586-024-07645-0

9 Zampaloni, C. *et al.* Author Correction: A novel antibiotic class targeting the lipopolysaccharide transporter. *Nature* **631**, E17 (2024). https://doi.org:10.1038/s41586-024-07641-4

10 Theuretzbacher, U. *et al.* Critical analysis of antibacterial agents in clinical development. *Nat Rev Microbiol* **18**, 286-298 (2020). https://doi.org:10.1038/s41579-020-0340-0

11 Brochado, A. R. *et al.* Species-specific activity of antibacterial drug combinations. *Nature* **559**, 259-263 (2018). https://doi.org:10.1038/s41586-018-0278-9

12 Cacace, E. *et al.* Systematic analysis of drug combinations against Gram-positive bacteria. *Nat Microbiol* **8**, 2196-2212 (2023). https://doi.org:10.1038/s41564-023-01486-9

13 Lehar, S. M. *et al.* Novel antibody-antibiotic conjugate eliminates intracellular S. aureus. *Nature* **527**, 323-328 (2015). https://doi.org:10.1038/nature16057

14 Tooke, C. L. *et al.* beta-Lactamases and beta-Lactamase Inhibitors in the 21st Century. *J Mol Biol* **431**, 3472-3500 (2019). https://doi.org:10.1016/j.jmb.2019.04.002

15 Imamovic, L. & Sommer, M. O. Use of collateral sensitivity networks to design drug cycling protocols that avoid resistance development. *Sci Transl Med* **5**, 204ra132 (2013). https://doi.org:10.1126/scitranslmed.3006609

16 Baym, M., Stone, L. K. & Kishony, R. Multidrug evolutionary strategies to reverse antibiotic resistance. *Science* **351**, aad3292 (2016). https://doi.org:10.1126/science.aad3292

17 Kim, S., Lieberman, T. D. & Kishony, R. Alternating antibiotic treatments constrain evolutionary paths to multidrug resistance. *Proc Natl Acad Sci U S A* **111**, 14494-14499 (2014). https://doi.org:10.1073/pnas.1409800111

18 Lazar, V. *et al.* Bacterial evolution of antibiotic hypersensitivity. *Mol Syst Biol* **9**, 700 (2013). https://doi.org:10.1038/msb.2013.57

19 Imamovic, L. *et al.* Drug-Driven Phenotypic Convergence Supports Rational Treatment Strategies of Chronic Infections. *Cell* **172**, 121-134 e114 (2018). https://doi.org:10.1016/j.cell.2017.12.012

20 Sakenova, N. *et al.* Systematic mapping of antibiotic cross-resistance and collateral sensitivity with chemical genetics. *Nat Microbiol* **10**, 202-216 (2025). https://doi.org:10.1038/s41564-024-01857-w

21 Andersson, D. I. & Levin, B. R. The biological cost of antibiotic resistance. *Curr Opin Microbiol* **2**, 489-493 (1999). https://doi.org:10.1016/s1369-5274(99)00005-3

22 Dunai, A. *et al.* Rapid decline of bacterial drug-resistance in an antibiotic-free environment through phenotypic reversion. *Elife* **8** (2019). https://doi.org:10.7554/eLife.47088

23 Norstrom, T., Lannergard, J. & Hughes, D. Genetic and phenotypic identification of fusidic acid-resistant mutants with the small-colony-variant phenotype in Staphylococcus aureus. *Antimicrob Agents Chemother* **51**, 4438-4446 (2007). https://doi.org:10.1128/AAC.00328-07

24 Spragge, F. *et al.* Microbiome diversity protects against pathogens by nutrient blocking. *Science* **382**, eadj3502 (2023). https://doi.org:10.1126/science.adj3502

25 Carlet, J. The gut is the epicentre of antibiotic resistance. *Antimicrob Resist Infect Control* **1**, 39 (2012). https://doi.org:10.1186/2047-2994-1-39

26 Raymond, F. *et al.* Culture-enriched human gut microbiomes reveal core and accessory resistance genes. *Microbiome* **7**, 56 (2019). https://doi.org:10.1186/s40168-019-0669-7

27 Wyres, K. L. *et al.* Genomic surveillance of antimicrobial resistant bacterial colonisation and infection in intensive care patients. *BMC Infect Dis* **21**, 683 (2021). https://doi.org:10.1186/s12879-021-06386-z

28 Garcia-Bayona, L. & Comstock, L. E. Bacterial antagonism in host-associated microbial communities. *Science* **361** (2018). https://doi.org:10.1126/science.aat2456

29 Culp, E. J. & Goodman, A. L. Cross-feeding in the gut microbiome: Ecology and mechanisms. *Cell Host Microbe* **31**, 485-499 (2023). https://doi.org:10.1016/j.chom.2023.03.016

30 Gordo, I., Perfeito, L. & Sousa, A. Fitness effects of mutations in bacteria. *J Mol Microbiol Biotechnol* **21**, 20-35 (2011). https://doi.org:10.1159/000332747

31 Bertagnolio, S. *et al.* WHO global research priorities for antimicrobial resistance in human health. *Lancet Microbe* **5**, 100902 (2024). https://doi.org:10.1016/S2666-5247(24)00134-4

32 Navon-Venezia, S., Kondratyeva, K. & Carattoli, A. Klebsiella pneumoniae: a major worldwide source and shuttle for antibiotic resistance. *FEMS Microbiol Rev* **41**, 252-275 (2017). https://doi.org:10.1093/femsre/fux013

33 Raffelsberger, N. *et al.* Gastrointestinal carriage of Klebsiella pneumoniae in a general adult population: a cross-sectional study of risk factors and bacterial genomic diversity. *Gut Microbes* **13**, 1939599 (2021). https://doi.org:10.1080/19490976.2021.1939599

34 Wong, J. L. C. *et al.* OmpK36-mediated Carbapenem resistance attenuates ST258 Klebsiella pneumoniae in vivo. *Nat Commun* **10**, 3957 (2019). https://doi.org:10.1038/s41467-019-11756-y

35 Garcia-Santamarina, S. *et al.* Emergence of community behaviors in the gut microbiota upon drug treatment. *Cell* **187**, 6346-6357 e6320 (2024). https://doi.org:10.1016/j.cell.2024.08.037

36 Griesshammer, A. *et al.* Non-antibiotics disrupt colonization resistance against enteropathogens. *Nature* **644**, 497-505 (2025). https://doi.org:10.1038/s41586-025-09217-2

37 Ruscheweyh, H. J. *et al.* mOTUs: Profiling Taxonomic Composition, Transcriptional Activity and Strain Populations of Microbial Communities. *Curr Protoc* **1**, e218 (2021). https://doi.org:10.1002/cpz1.218

38 Tenaillon, O., Skurnik, D., Picard, B. & Denamur, E. The population genetics of commensal Escherichia coli. *Nat Rev Microbiol* **8**, 207-217 (2010). https://doi.org:10.1038/nrmicro2298

39 Galardini, M. *et al.* Phenotype inference in an *Escherichia coli* strain panel. *Elife* **6** (2017). https://doi.org:10.7554/eLife.31035

40 Andersen, C., Krones, D., Ulmke, C., Schmid, K. & Benz, R. The porin RafY encoded by the raffinose plasmid pRSD2 of Escherichia coli forms a general diffusion pore and not a carbohydrate-specific porin. *Eur J Biochem* **254**, 679-684 (1998). https://doi.org:10.1046/j.1432-1327.1998.2540679.x

41 Ulmke, C., Lengeler, J. W. & Schmid, K. Identification of a new porin, RafY, encoded by raffinose plasmid pRSD2 of Escherichia coli. *J Bacteriol* **179**, 5783-5788 (1997). https://doi.org:10.1128/jb.179.18.5783-5788.1997

42 Nikaido, H. Molecular basis of bacterial outer membrane permeability revisited. *Microbiology and molecular biology reviews : MMBR* **67**, 593-656 (2003).

43 Dunstan, R. A. *et al.* Epitopes in the capsular polysaccharide and the porin OmpK36 receptors are required for bacteriophage infection of Klebsiella pneumoniae. *Cell Rep* **42**, 112551 (2023). https://doi.org:10.1016/j.celrep.2023.112551

44 Low, W. W. *et al.* Mating pair stabilization mediates bacterial conjugation species specificity. *Nat Microbiol* **7**, 1016-1027 (2022). https://doi.org:10.1038/s41564-022-01146-4

45 Savitski, M. M. *et al.* Tracking cancer drugs in living cells by thermal profiling of the proteome. *Science* **346**, 1255784 (2014). https://doi.org:10.1126/science.1255784

46 Mateus, A. *et al.* Thermal proteome profiling in bacteria: probing protein state *in vivo*. *Mol Syst Biol* **14**, e8242 (2018). https://doi.org:10.15252/msb.20188242

47 Mateus, A. *et al.* The functional proteome landscape of Escherichia coli. *Nature* **588**, 473-478 (2020). https://doi.org:10.1038/s41586-020-3002-5

48 Eberl, C. *et al. E. coli* enhance colonization resistance against *Salmonella* Typhimurium by competing for galactitol, a context-dependent limiting carbon source. *Cell host & microbe* **29**, 1680-1692 e1687 (2021). https://doi.org:10.1016/j.chom.2021.09.004

49 Osbelt, L. *et al.* Klebsiella oxytoca causes colonization resistance against multidrug-resistant K. pneumoniae in the gut via cooperative carbohydrate competition. *Cell Host Microbe* **29**, 1663-1679 e1667 (2021). https://doi.org:10.1016/j.chom.2021.09.003

50 Oliveira, R. A. *et al.* Klebsiella michiganensis transmission enhances resistance to Enterobacteriaceae gut invasion by nutrition competition. *Nat Microbiol* **5**, 630-641 (2020). https://doi.org:10.1038/s41564-019-0658-4

51 Woelfel, S., Silva, M. S. & Stecher, B. Intestinal colonization resistance in the context of environmental, host, and microbial determinants. *Cell Host Microbe* **32**, 820-836 (2024). https://doi.org:10.1016/j.chom.2024.05.002

52 Almasi, E. D. H. *et al.* Klebsiella oxytoca facilitates microbiome recovery via antibiotic degradation and restores colonization resistance in a diet-dependent manner. *Nat Commun* **16**, 551 (2025). https://doi.org:10.1038/s41467-024-55800-y

53 Forage, R. G. & Foster, M. A. Glycerol fermentation in Klebsiella pneumoniae: functions of the coenzyme B12-dependent glycerol and diol dehydratases. *J Bacteriol* **149**, 413-419 (1982). https://doi.org:10.1128/jb.149.2.413-419.1982

54 Raynaud, C., Sarcabal, P., Meynial-Salles, I., Croux, C. & Soucaille, P. Molecular characterization of the 1,3-propanediol (1,3-PD) operon of Clostridium butyricum. *Proc Natl Acad Sci U S A* **100**, 5010-5015 (2003). https://doi.org:10.1073/pnas.0734105100

55 Guo, Y. *et al.* 1,3-Propanediol production by a newly isolated strain, Clostridium perfringens GYL. *Bioresour Technol* **233**, 406-412 (2017). https://doi.org:10.1016/j.biortech.2017.02.116

56 Weirauch, T., Yahav, D., Zahavi, I., Wurstle, S. & Vehreschild, M. A review on antibiotic and non-antibiotic decolonization strategies of multidrug-resistant bacteria in the gastrointestinal tract. *Infection* (2026). https://doi.org:10.1007/s15010-025-02718-2

57 Muller, P. *et al.* High-throughput anaerobic screening for identifying compounds acting against gut bacteria in monocultures or communities. *Nat Protoc* **19**, 668-699 (2024). https://doi.org:10.1038/s41596-023-00926-4

58 Murali, A., Bhargava, A. & Wright, E. S. IDTAXA: a novel approach for accurate taxonomic classification of microbiome sequences. *Microbiome* **6**, 140 (2018). https://doi.org:10.1186/s40168-018-0521-5

59 Dmitrijeva, M. *et al.* The mOTUs online database provides web-accessible genomic context to taxonomic profiling of microbial communities. *Nucleic Acids Res* **53**, D797-D805 (2025). https://doi.org:10.1093/nar/gkae1004

60 Datsenko, K. A. & Wanner, B. L. One-step inactivation of chromosomal genes in Escherichia coli K-12 using PCR products. *Proc Natl Acad Sci U S A* **97**, 6640-6645 (2000). https://doi.org:10.1073/pnas.120163297

61 Datta, S., Costantino, N. & Court, D. L. A set of recombineering plasmids for gram-negative bacteria. *Gene* **379**, 109-115 (2006). https://doi.org:10.1016/j.gene.2006.04.018

62 Argimon, S. *et al.* Rapid Genomic Characterization and Global Surveillance of Klebsiella Using Pathogenwatch. *Clin Infect Dis* **73**, S325-S335 (2021). https://doi.org:10.1093/cid/ciab784

63 Danecek, P. *et al.* Twelve years of SAMtools and BCFtools. *Gigascience* **10** (2021). https://doi.org:10.1093/gigascience/giab008

64 Croucher, N. J. *et al.* Rapid phylogenetic analysis of large samples of recombinant bacterial whole genome sequences using Gubbins. *Nucleic Acids Res* **43**, e15 (2015). https://doi.org:10.1093/nar/gku1196

65 Kozlov, A. M., Darriba, D., Flouri, T., Morel, B. & Stamatakis, A. RAxML-NG: a fast, scalable and user-friendly tool for maximum likelihood phylogenetic inference. *Bioinformatics* **35**, 4453-4455 (2019). https://doi.org:10.1093/bioinformatics/btz305

66 Lam, M. M. C. *et al.* A genomic surveillance framework and genotyping tool for Klebsiella pneumoniae and its related species complex. *Nat Commun* **12**, 4188 (2021). https://doi.org:10.1038/s41467-021-24448-3

67 Camacho, C. *et al.* BLAST+: architecture and applications. *BMC Bioinformatics* **10**, 421 (2009). https://doi.org:10.1186/1471-2105-10-421

68 Gouy, M., Tannier, E., Comte, N. & Parsons, D. P. Seaview Version 5: A Multiplatform Software for Multiple Sequence Alignment, Molecular Phylogenetic Analyses, and Tree Reconciliation. *Methods Mol Biol* **2231**, 241-260 (2021). https://doi.org:10.1007/978-1-0716-1036-7_15

69 Argimon, S. *et al.* Microreact: visualizing and sharing data for genomic epidemiology and phylogeography. *Microb Genom* **2**, e000093 (2016). https://doi.org:10.1099/mgen.0.000093

70 Carver, T. J. *et al.* ACT: the Artemis Comparison Tool. *Bioinformatics* **21**, 3422-3423 (2005). https://doi.org:10.1093/bioinformatics/bti553

71 Assefa, S., Keane, T. M., Otto, T. D., Newbold, C. & Berriman, M. ABACAS: algorithm-based automatic contiguation of assembled sequences. *Bioinformatics* **25**, 1968-1969 (2009). https://doi.org:10.1093/bioinformatics/btp347

72 Montenegro-Burke, J. R., Guijas, C. & Siuzdak, G. METLIN: A Tandem Mass Spectral Library of Standards. *Methods Mol Biol* **2104**, 149-163 (2020). https://doi.org:10.1007/978-1-0716-0239-3_9

73 Wishart, D. S. *et al.* HMDB 5.0: the Human Metabolome Database for 2022. *Nucleic Acids Res* **50**, D622-D631 (2022). https://doi.org:10.1093/nar/gkab1062

74 Dricot, C. E. M. K. *et al.* Vitamin B₂ Production by Vaginal Lactobacilli Promotes Symbiosis. *bioRxiv*, 2025.2010.2028.684342 (2025). https://doi.org:10.1101/2025.10.28.684342

75 B, B. preprocessCore: a collection of pre-processing functions. R package version 1.64.0. https://bioconductor.org/packages/preprocessCore. (2025). https://doi.org:doi:10.18129/B9.bioc.preprocessCore

76 Klunemann, M. *et al.* Bioaccumulation of therapeutic drugs by human gut bacteria. *Nature* **597**, 533-538 (2021). https://doi.org:10.1038/s41586-021-03891-8

77 Hughes, C. S. *et al.* Single-pot, solid-phase-enhanced sample preparation for proteomics experiments. *Nat Protoc* **14**, 68-85 (2019). https://doi.org:10.1038/s41596-018-0082-x

78 Franken, H. *et al.* Thermal proteome profiling for unbiased identification of direct and indirect drug targets using multiplexed quantitative mass spectrometry. *Nat Protoc* **10**, 1567-1593 (2015). https://doi.org:10.1038/nprot.2015.101

79 Kong, A. T., Leprevost, F. V., Avtonomov, D. M., Mellacheruvu, D. & Nesvizhskii, A. I. MSFragger: ultrafast and comprehensive peptide identification in mass spectrometry-based proteomics. *Nat Methods* **14**, 513-520 (2017). https://doi.org:10.1038/nmeth.4256

80 Huber, W., von Heydebreck, A., Sultmann, H., Poustka, A. & Vingron, M. Variance stabilization applied to microarray data calibration and to the quantification of differential expression. *Bioinformatics* **18 Suppl 1**, S96-104 (2002). https://doi.org:10.1093/bioinformatics/18.suppl_1.s96

81 Becher, I. *et al.* Pervasive Protein Thermal Stability Variation during the Cell Cycle. *Cell* **173**, 1495-1507 e1418 (2018). https://doi.org:10.1016/j.cell.2018.03.053

82 Ritchie, M. E. *et al.* limma powers differential expression analyses for RNA-sequencing and microarray studies. *Nucleic Acids Res* **43**, e47 (2015). https://doi.org:10.1093/nar/gkv007

1127 Figures with legends

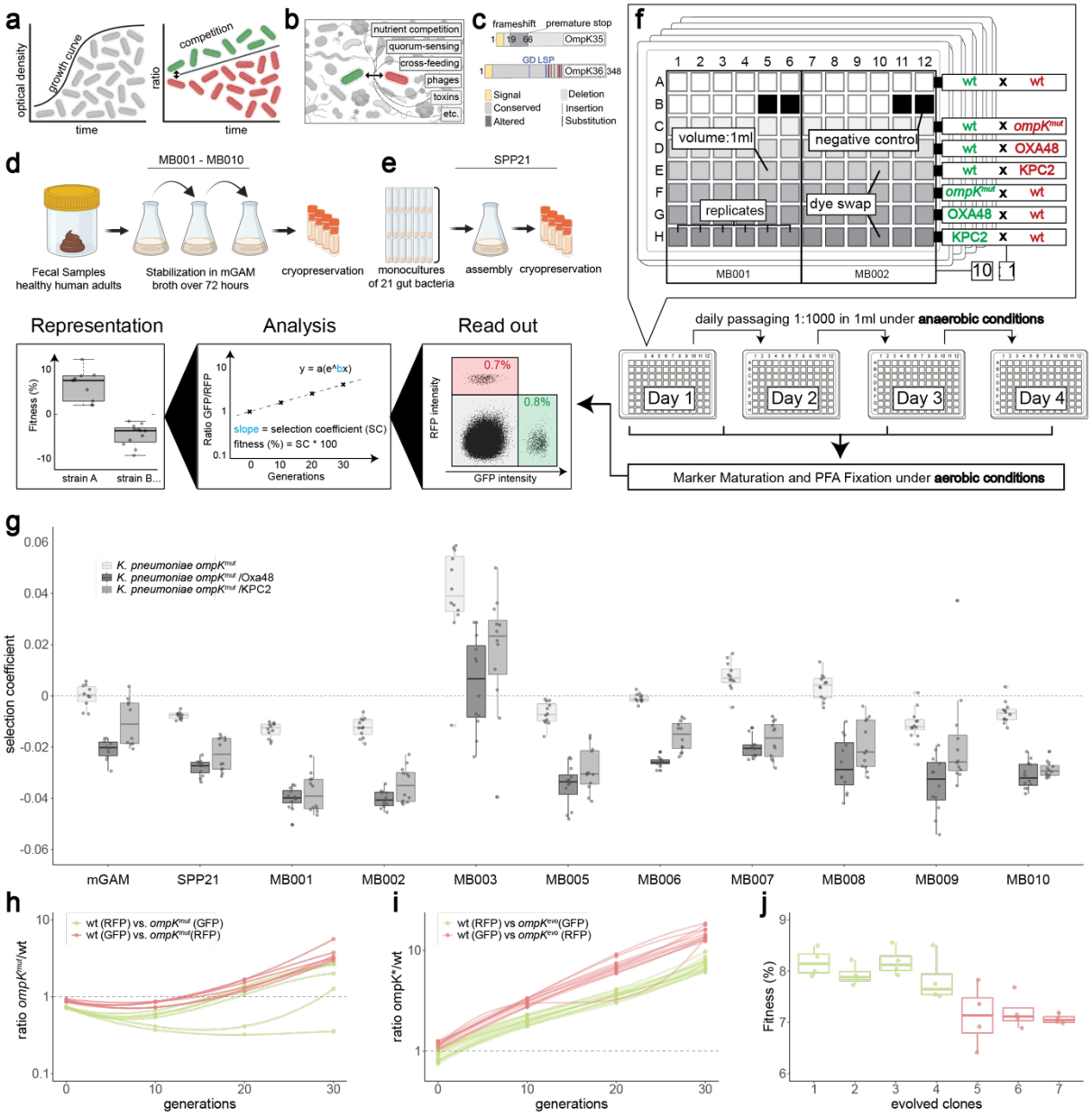

1128

1129 **Figure 1 – A sensitive method for identifying specific microbiotas that (counter-)select for**
1130 **an antibiotic resistant *K. pneumoniae* mutant. a,** Conventional methods to determine
1131 bacterial fitness *in vitro*. Fitness is measured by determining lag time, exponential growth rate
1132 and maximum yield of an axenically grown culture, or by competing two differently tagged
1133 isogenic strains over time to determine their change in ratios, and thereby the selection
1134 coefficient. **b,** Schematic representation of factors influencing bacterial fitness in complex
1135 communities. **c,** Mutations present in the *K. pneumoniae* porin mutant. *ompK35* carries a
1136 frameshift mutation resulting in a premature stop after 66 amino acids causing a complete
1137 loss of function. *ompK*36 carries a series of clinically prevalent mutations including a GD-

1138 insertion resulting in a restriction of the pore diameter. **d,** Preparation of cryopreserved stool-
1139 derived microbial communities MB001 to MB010. Fecal samples of healthy human adults
1140 were mixed 1:1 with PBS and diluted in mGAM broth, passaged anaerobically for 3 days in
1141 fresh medium and cryopreserved in presence of 12.5% glycerol. **e,** Preparation of
1142 cryopreserved synthetic community SPP21. Overnight cultures of 21 prevalent gut bacterial
1143 species mixed at equimolar ratios. The synthetic community was grown overnight and
1144 cryopreserved in presence of 12.5% glycerol. **f,** Experimental setup of the competition
1145 experiment between various antibiotic-resistant *K. pneumoniae* strains in presence of
1146 different human gut microbiomes. Both stool-derived and synthetic communities were
1147 passaged twice after reviving from glycerol and before competition started. Competitions
1148 were performed in 96 deep-well plates with daily passing over 3-4 days under anaerobic
1149 conditions with the indicated experimental parameters. Maturation of the fluorescent
1150 proteins, PFA-fixation and readout using flow cytometry were performed aerobically. **g,**
1151 Selection coefficients of *K. pneumoniae ompK35/ompK36* mutant (annotated as *K.*
1152 *pneumoniae ompK*^{mut}) with or without OXA48 or KPC-2 compared to an isogenic wildtype
1153 strain in absence (mGAM) or presence of 10 different fecal or synthetic microbiomes. All
1154 competitions were performed in a minimum of 5 replicates per marker combination, and all
1155 resistant mutant were competed against the wild type with GFP and RFP (with the mutant
1156 carrying the corresponding complementary marker). The GFP or RFP associated fitness cost
1157 was determined in a wildtype versus wildtype competition and used for subsequent
1158 correction of selection coefficients (see methods). Center lines show the medians; box limits
1159 indicate the 25th and 75th percentiles; whiskers extend 1.5 times the interquartile range from
1160 the 25th and 75th percentiles, data points are plotted as dots. **h,** Change in ratio of *ompK*^{mut}
1161 over *K. pneumoniae* wildtype in presence of MB003 over 4 days. Colors indicate the marker
1162 carried by the porin mutant. **i,** Change in ratio of *K. pneumoniae ompK*^{evo} over the wildtype in
1163 presence of MB003 over 4 days. Colors indicate if the evolved mutant was isolated from the
1164 GFP- or RFP-tagged lineage of *ompK*^{mut} **j,** Selection coefficient of seven *K. pneumoniae ompK*^{evo}
1165 endpoint clones over the wildtype in presence of MB003. The selection coefficients were
1166 corrected for the marker cost determined by the wildtype-wildtype competition in presence
1167 of MB003. Colors as in panel **i**.

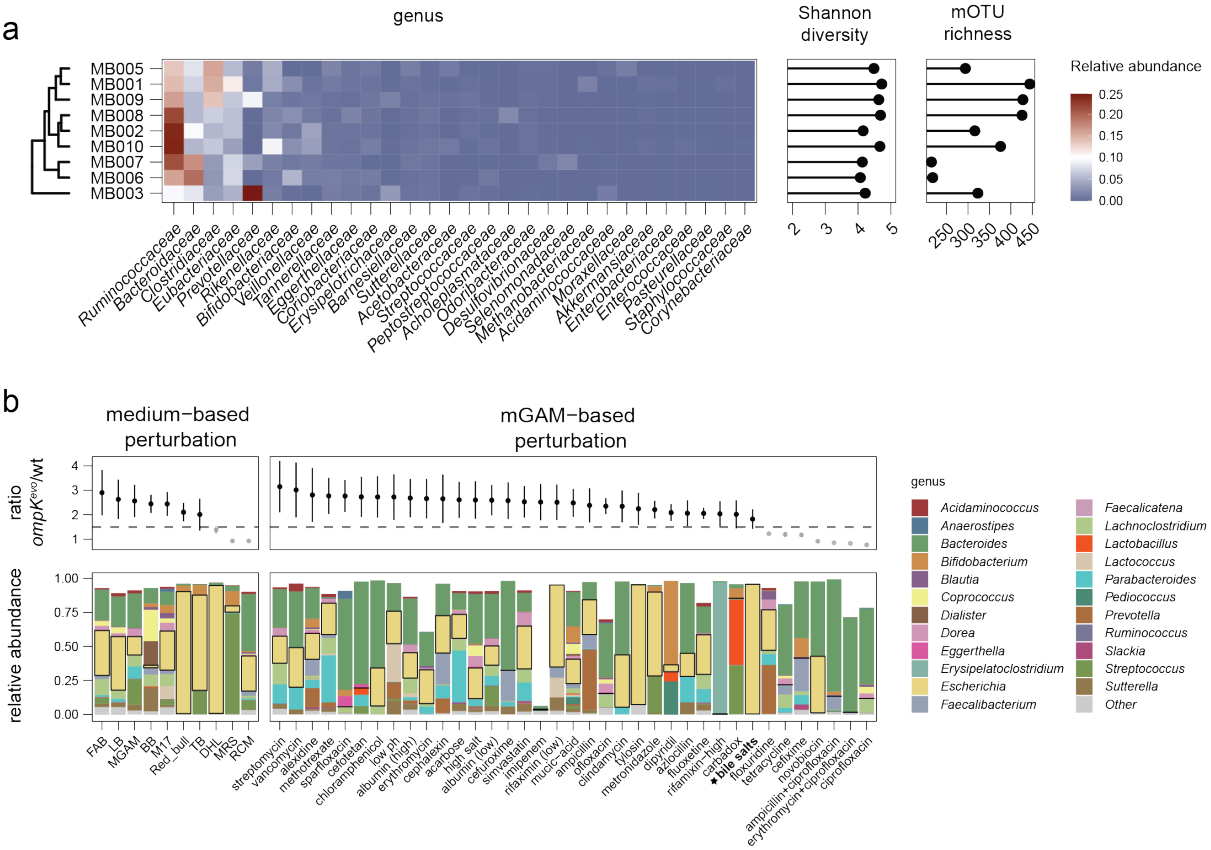

Figure 2 – Identification of Microbiome MB003 community members driving the enrichment of *K. pneumoniae ompK^evo^*. a, Composition, Shannon diversity and mOTU richness of the fecal derived communities MB001-MB010 based on metagenomic analysis (see methods). **b,** Ratio of *K. pneumoniae ompK^evo^* over the wildtype after one day of co-culture in different MB003-derived subcommunities. The subcommunities were generated by daily passaging of MB003 under various selective conditions for 3 days. The data points in the upper panel (n = 4 replicates, error bars represent standard deviation) correspond to relative abundance of *K. pneumoniae ompK^evo^* over the wildtype after passaging a 1:1 mixture in the subcommunities for 24hours (secondary y axis). The lower panel shows the microbial composition based on 16S rRNA sequencing. *Escherichia* abundance is accentuated with a black outline.

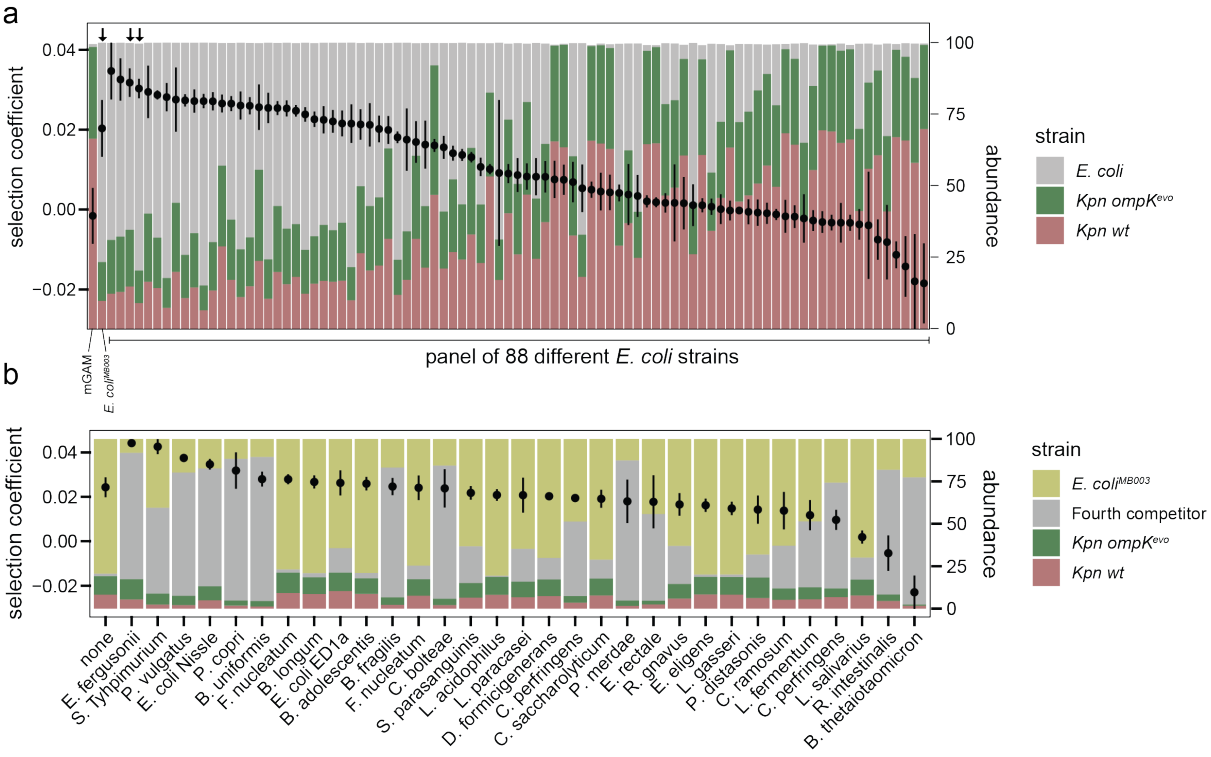

Figure 3 – The selective advantage of *K. pneumoniae ompK^{evo}* is driven by many *E. coli* strains and depends on higher-order interactions with other gut bacteria. a, Selective advantage of *K. pneumoniae ompK^{evo}* over the wildtype in the presence of different *E. coli* strains. The competitions were performed with each *E. coli* strain individually (triple competitions). Data points (primary y-axis) represent the average selection coefficient of *K. pneumoniae ompK^{evo}* over the wildtype of four replicates. Error bars represent the standard deviation. The stacked bars (secondary y-axis) represent abundance of the indicated strains at the end point of the competition experiment as determined by flow cytometry. Arrows above bars indicate *E. coli* strains that were isolated from the fecal microbiomes MB003, MB001 and MB005 (left to right). **b,** Selective advantage of *K. pneumoniae ompK^{evo}* over the wildtype in presence of YFP-labelled *E. coli^{MB003}* and various fourth competitors. The competitions were performed in presence of each fourth competitor individually (quadruple competitions). Data representation as in panel **a**.

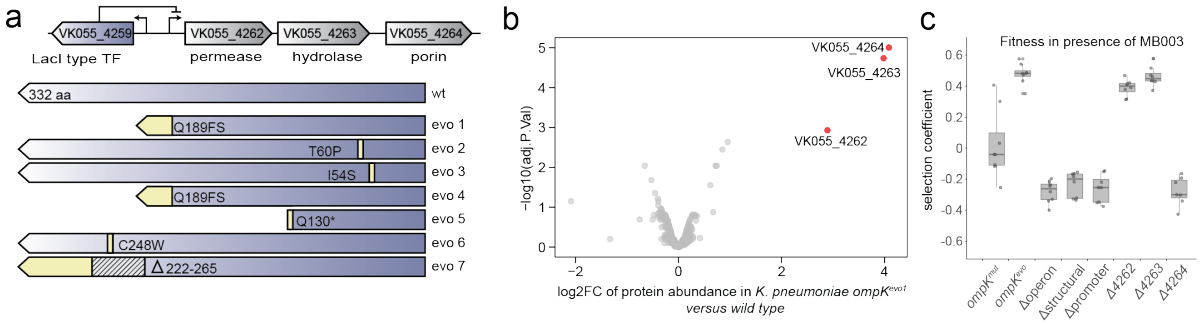

Figure 4 – Mutations in a transcription factor in *K. pneumoniae ompK^{evo}* cause the fitness advantage in MB003, due to upregulation of the downstream porin. a, Whole genome sequence analysis of seven *K. pneumoniae ompK^{evo}* mutants. All clones carry mutations in a LacI-type transcription factor resulting in premature stops, internal deletions or amino acid substitutions. The transcription factor is located upstream of a carbohydrate catabolic operon consisting of a permease, a hydrolase and an additional porin. The labels indicate the locus tags according to reference genome CP009208. **b,** Proteome abundance changes induced by acquisition of a *glyR* mutation in *K. pneumoniae ompK^{mut}*. The wildtype and evolved porin mutant carrying a T60P substitution in the LacI-type transcription factor (evo2) were grown for 16 hours in mGAM under anaerobic conditions and subjected to mass spectrometry. All genes of the carbohydrate catabolic operon are upregulated in the *glyR* T60P mutant. **c,** Selective advantage of various deletion mutants of the carbohydrate-catabolic operon in the *K. pneumoniae ompK^{evo}* background or in the wildtype background over the parental strain in presence of MB003. Upregulation of the porin (4264) is causal for the observed selective advantage. Box plots are depicted as in Fig. 1g.

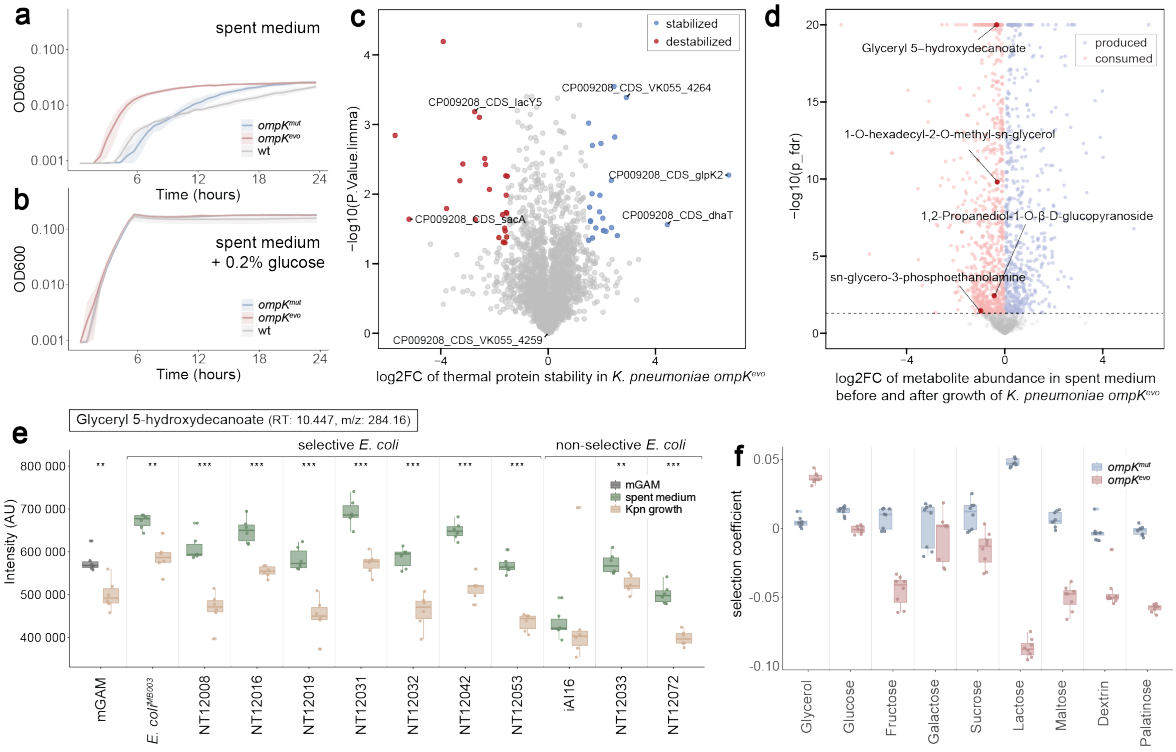

Figure 5 – GlyP upregulation allows *K. pneumoniae* to benefit from glycerol containing compounds. a, Growth curves of *K. pneumoniae* wildtype, *ompK*^{mut} and *ompK*^{evo} in *E. coli*^{MB003} spent medium without supplements or **b,** with supplementation of 0.2% glucose. The spent medium was prepared by growing *E. coli*^{MB003} overnight in mGAM at 37 °C under anaerobic conditions and subsequent sterile filtration with a 0.22µM pore size filter. Lines represent average of four independent replicates, confidence intervals represent one standard deviation. **c,** Change in thermal stability of the proteome of *K. pneumoniae ompK*^{evo} compared to the wildtype in presence of *E. coli*^{MB003} spent medium (see methods). Three replicates of *K. pneumoniae ompK*^{evo} and *K. pneumoniae* wild type were grown anaerobically overnight in mGAM. Whole-cells lysates were treated with *E. coli*^{MB003} spent medium and subjected to thermal proteome profiling. Significant hits are indicated with red (destabilized) and blue (stabilized). Members of the carbohydrate catabolic operon described in **Fig. 4a** as well as the two strongest stabilized proteins are labelled. **d,** Metabolomics of *E. coli*^{MB003} spent medium before and after growth of *K. pneumoniae ompK*^{evo}. Compounds significantly enriched after growth of *K. pneumoniae ompK*^{evo} are colored in blue, compounds significantly diminished are coloured in red. Glycerol-derivatives are labelled. **e**, Signal intensities for Glyceryl 5-hydroxydecanoate in spent media of seven different *E. coli* isolates and in mGAM before and after growth of *K pneumoniae ompK*^{evo}. All experiments were performed in six replicates. Box

1229 plots depicted as in Fig. 1g. Statistical significance was assessed using a t-test. * $p_{adjusted} < 0.05$,
1230 ** $p_{adjusted} < 0.01$, *** $p_{adjusted} < 0.001$ **f**, Fitness of *K. pneumoniae ompK*^{mut} and *K. pneumoniae*
1231 *ompK*^{evo} compared to *K. pneumoniae* wildtype grown in different carbon sources.
1232 Competitions were performed in M9 minimal media supplemented with defined carbon
1233 sources as indicated. Box plots are depicted as in Fig. 1g.
1234
1235

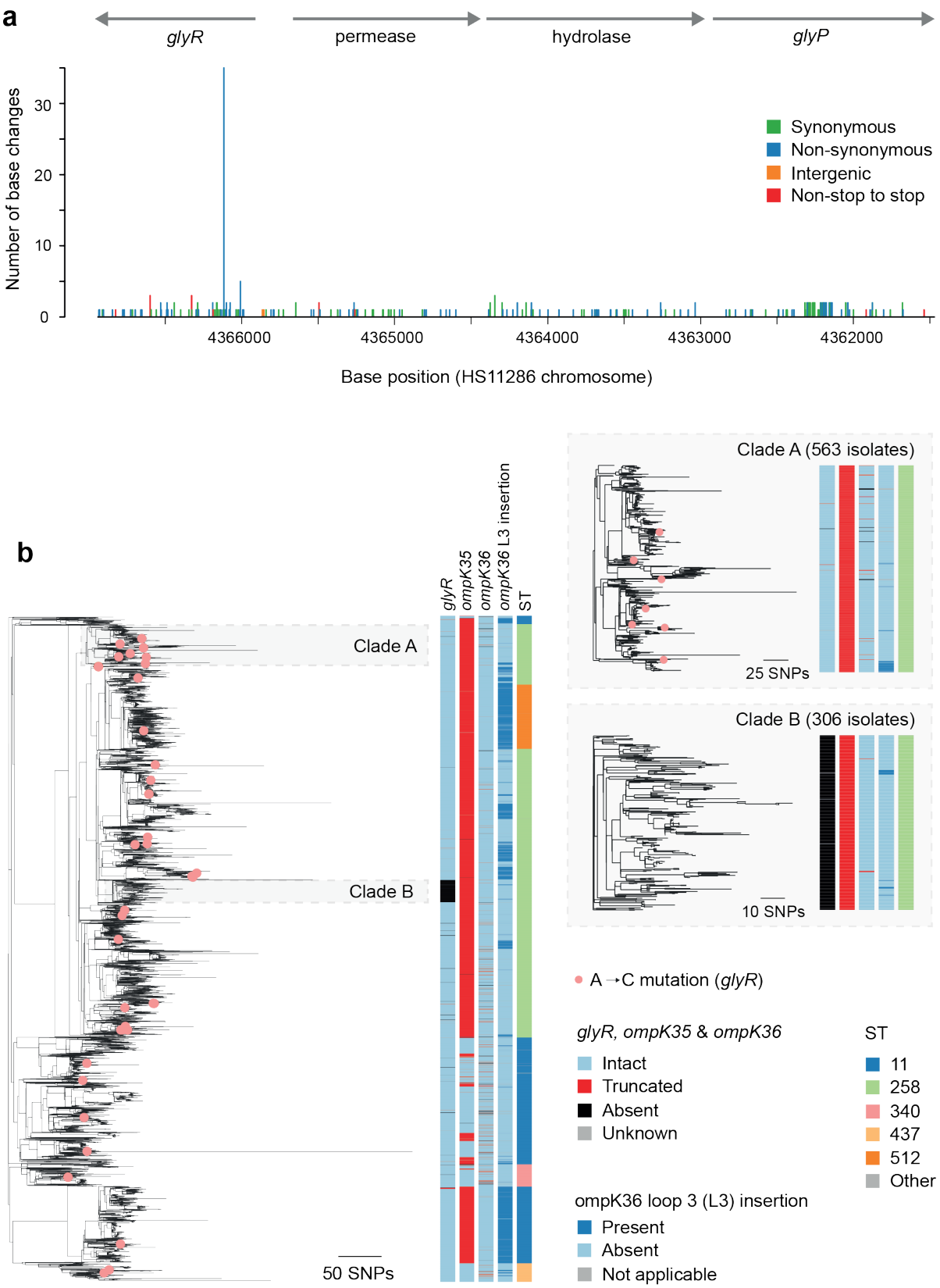

Figure 6 - *glyR* T60P substitution is under conditional positive selection in clinical isolates of *K. pneumoniae*. a, Number of base (state) changes inferred to have occurred across the phylogeny of 9214 CC258 isolates at each base position spanning the length of the *glyR*/*glyP*

1240 operons and with respect to the HS11286 reference genome. Base changes are colored by
1241 their effect on the protein sequence. **b**, Phylogenetic tree of 9214 CC258 isolates constructed
1242 after the removal of recombined regions from the alignment. Isolate nodes are colored pink
1243 if they possess a "C" at position 4366094 (with respect to the HS11286 reference),
1244 corresponding to amino acid position 60 within the LacI type TF. Metadata columns show
1245 whether the *glyR*, *ompK35* and *ompK36* genes are intact, truncated or absent, the presence
1246 or absence of an *ompK36* loop 3 insertion (GD or TD) and the ST of the genomes. Clades A and
1247 B are shown with additional resolution on the right-hand side. The scale bars represent the
1248 number of SNPs. An interactive vizualisation of this tree, together with additional metadata
1249 and genotypic data, is available via Microreact at https://microreact.org/project/kp-cc258.
1250
1251

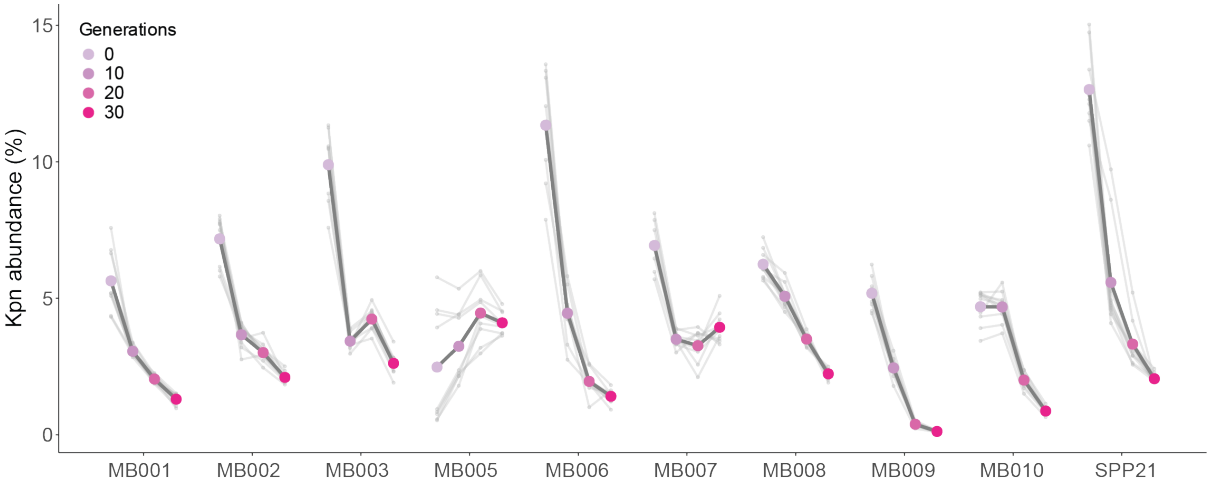

Extended Data Fig. 1: Abundance of *K. pneumoniae* wildtype in different microbiomes over the course of the competition experiment. Dark grey lines show the mean total abundance of the *K. pneumoniae* competitors in various fecal derived and synthetic microbiomes, whereas light grey lines indicate abundance in each replicate. Abundancies were determined by flow cytometry, where GFP^+ and RFP^+ cells represented *K. pneumoniae* and nonfluorescent events represent community members. Competitions were passaged for 4 days in mGAM under anaerobic conditions at 37 °C with a daily dilution factor of 1:1000 corresponding to about 10 generations of growth per day.

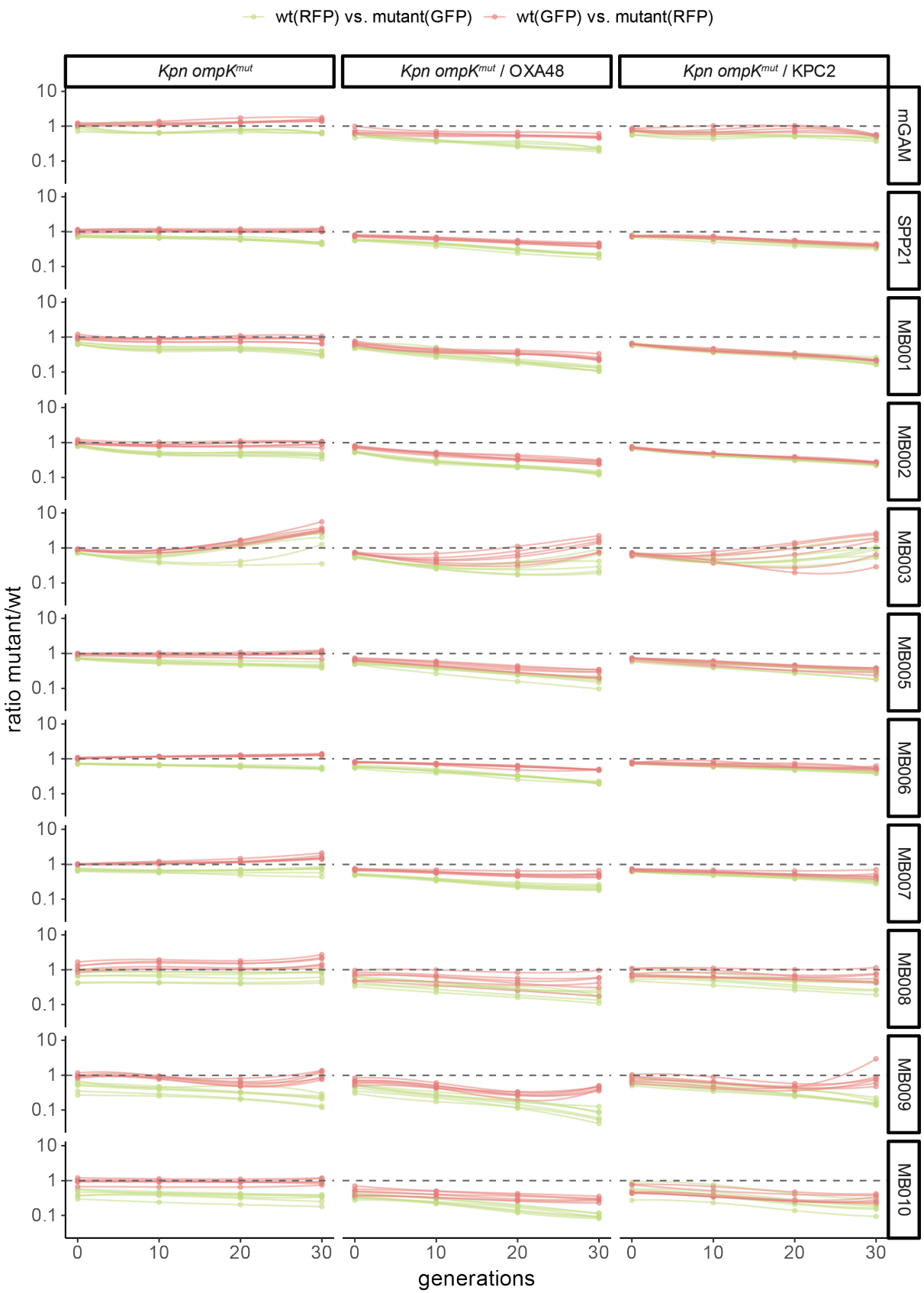

1262

1263 **Extended Data Fig. 2: Change in ratios over time of *K. pneumoniae* competitors in presence**

1264 **and absence of various communities.** Green and red data points represent competitions

1265 where the resistant mutant (*K. pneumoniae ompK*^{mut}*, ompK*^{mut} /pOXA48 *and ompK*^{mut} /KPC2)
1266 was tagged with GFP or RFP, respectively. Ratios were determined daily by flow cytometry.
1267 Competitions were performed as described in Extended Data Fig. 1.
1268

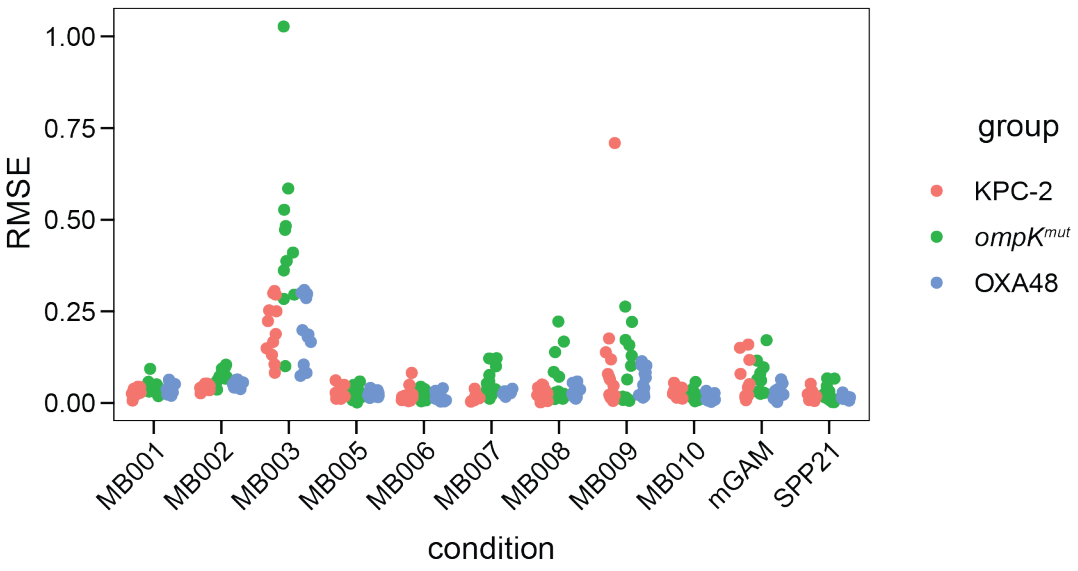

Extended Data Fig. 3: Fit measures for selection coefficients. Root mean squared error (RSME) of linear models fits of change in ratios of indicated *K. pneumoniae* strain over the wildtype as a function of time in different community compositions. Each datapoint represents the RSME of an individual replicate of a longitudinal fitness experiment. Corresponds to curves shown in Extended Data Fig. 2

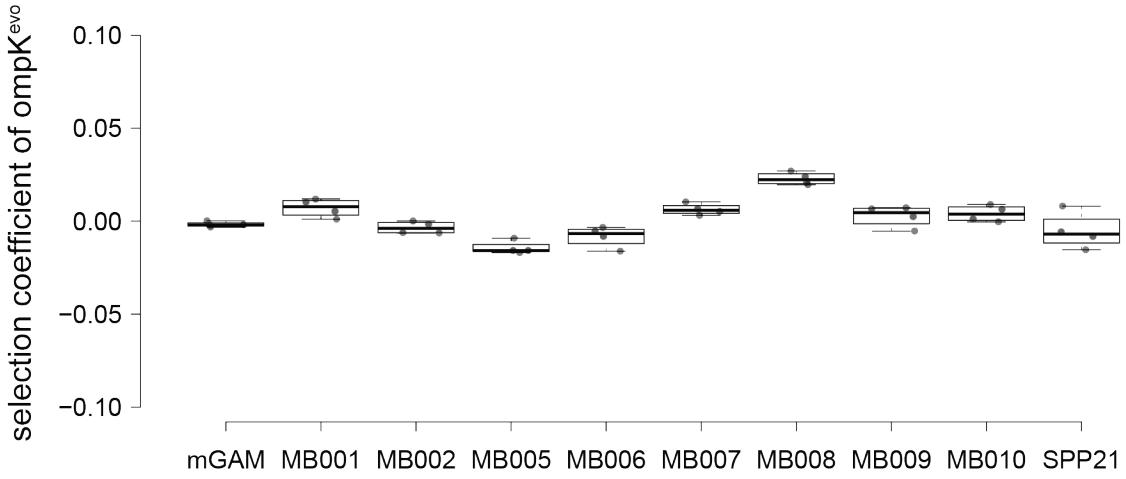

Extended Data Fig. 4: Selection coefficient of *K. pneumoniae ompK^{evo}* in different microbiomes. *K. pneumoniae ompK^{evo}* GFP^{+} was competed with an RFP^{+} *K. pneumoniae* wildtype over 4 days using the previously described competition setup in presence or absence of different microbial communities. Box plots are depicted as in Fig. 1g (n is minimum of four biological replicates).

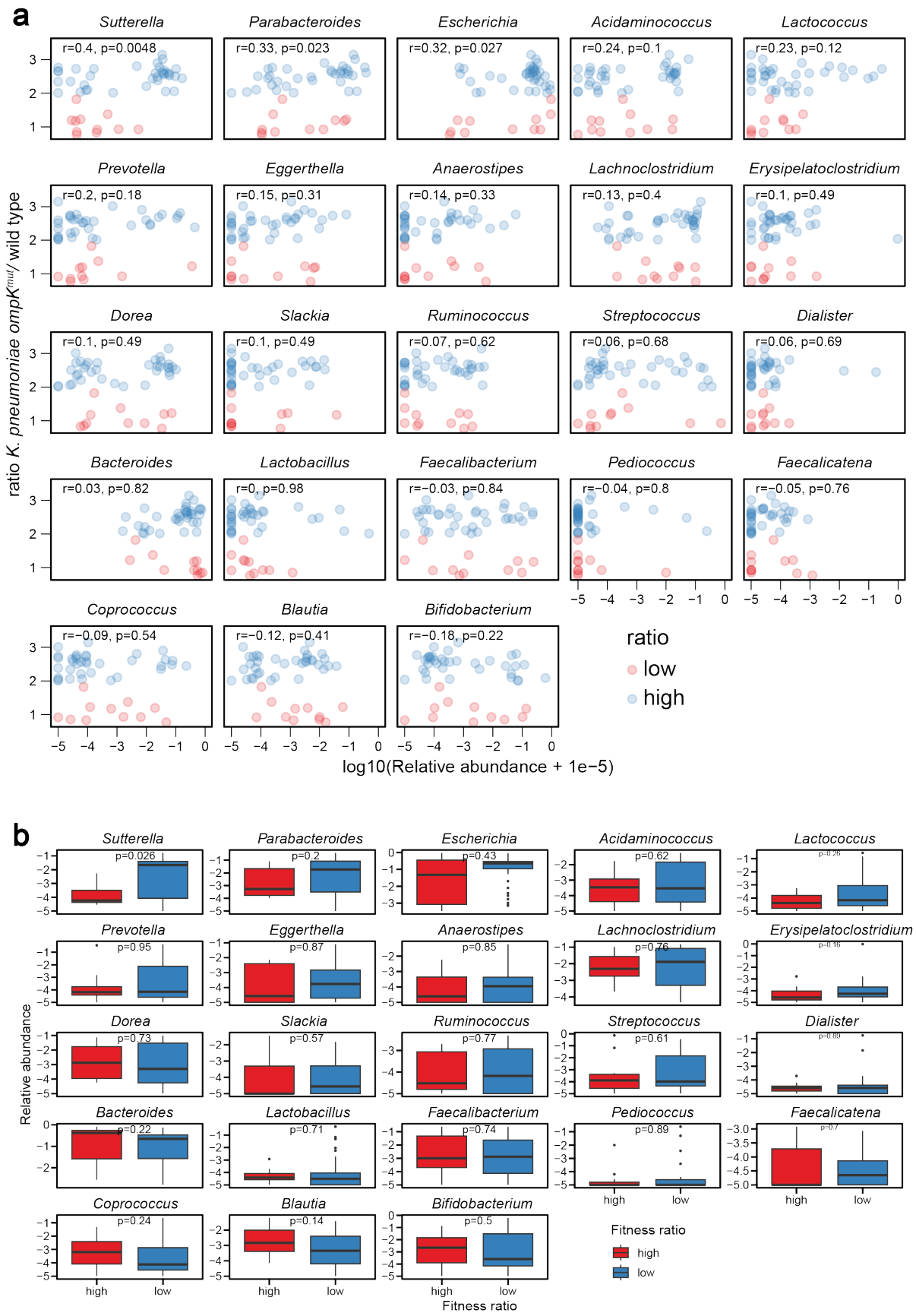

Extended Data Fig. 5: MB003 subcommunity selection of *K. pneumoniae ompK*^{evo} over *K. pneumoniae*. a, Scatter plot of *K. pneumoniae ompK*^{evo} over wildtype ratios against taxon

1286 relative abundances in microbiome MB003 derived subcommunities. Relative abundances of
1287 taxa are log10-scaled. Conditions are grouped into high and low fitness ratios, where
1288 conditions that enriched *K. pneumoniae ompK*^{evo} over wildtype at least 2-fold are considered
1289 high, everything below as low. P-values were computed using a Pearson correlation test. Only
1290 genera with a relative abundance of at least 5% in at least one of the perturbation conditions
1291 are shown. **b,** Box plot of taxon relative abundances between high fitness ratio and low fitness
1292 ratio perturbation conditions. Relative abundances of taxa are log10-scaled**.** Conditions are
1293 grouped into high and low fitness. P-values were computed using a Wilcoxon rank-sum test.
1294 Only genera with a relative abundance of at least 5% in at least one of the perturbation
1295 conditions are shown.
1296

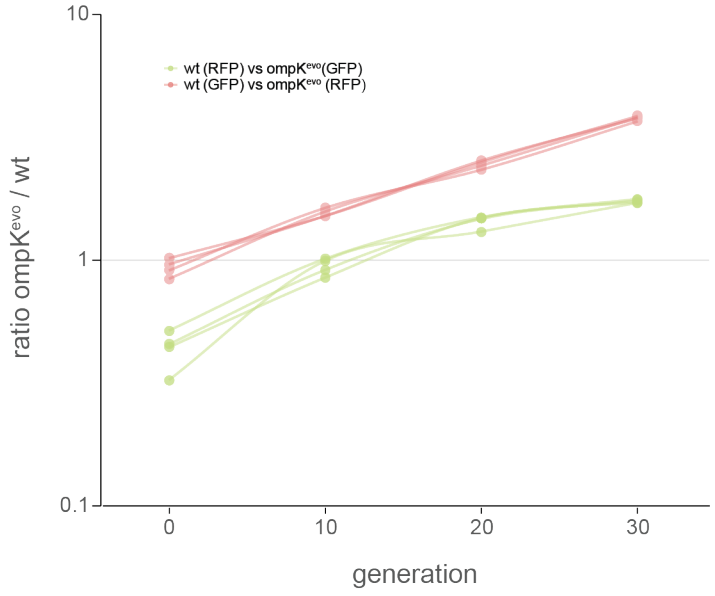

1297

1298 **Extended Data Fig. 6: Ratio of *K. pneumoniae ompK^{evo}* over the wildtype in the presence of**

1299 ***E. coli^{MB003}* over 40 generations of growth.** Each line represents a replicate competition and

1300 colors indicate the marker carried by the porin mutant (green = GFP, red = RFP)

1301

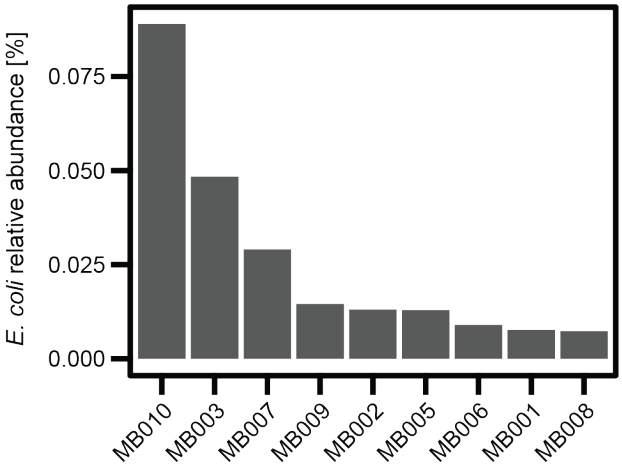

1302

1303 **Extended Data Fig. 7: Abundance of *E. coli* in native stool samples from MB001-MB010.** This

1304 is based on metagenomics analysis of MB001-MB010 shown in Fig. 2a.

1305

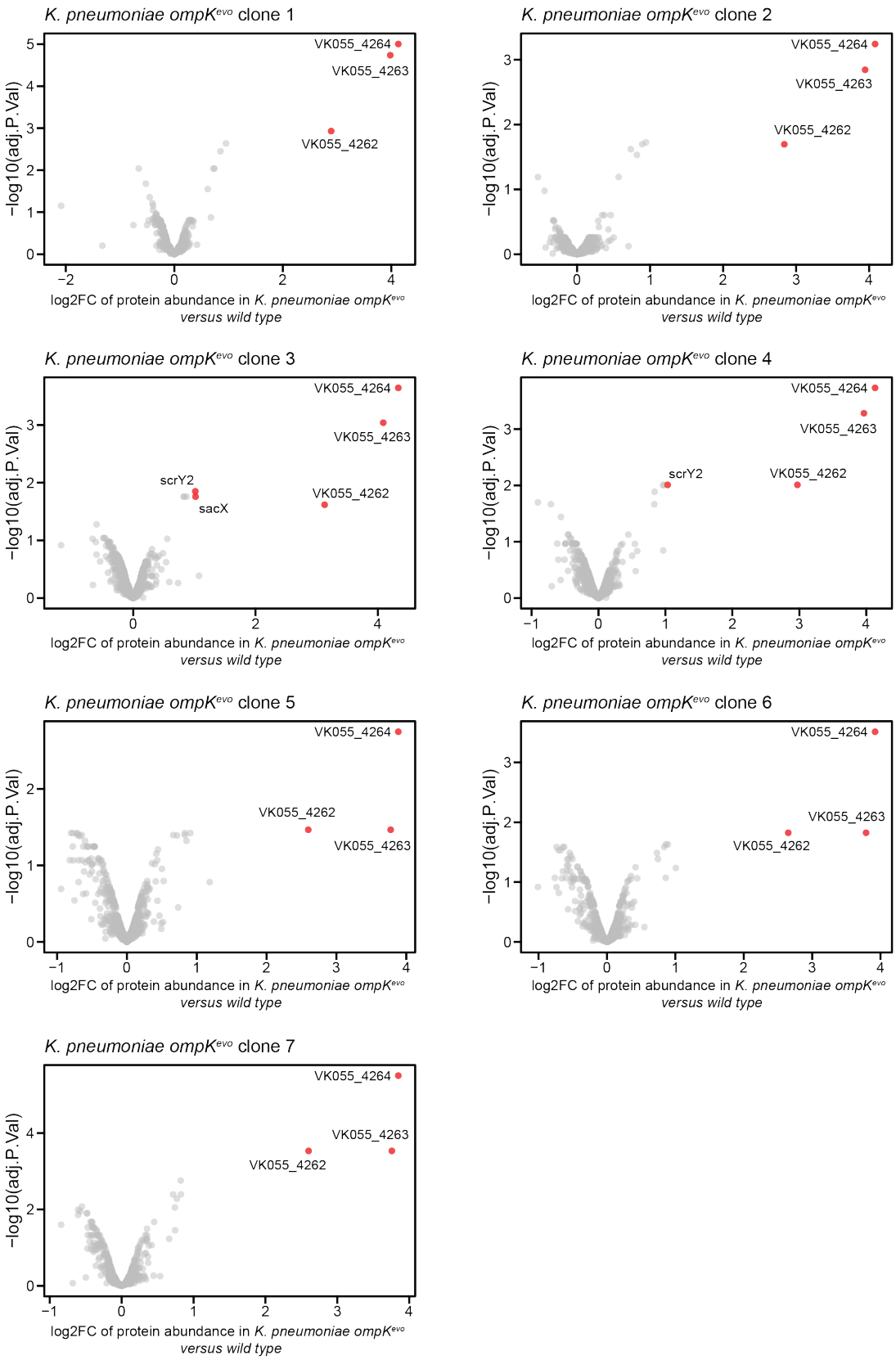

Extended Data Fig. 8: Protein abundance changes in *K. pneumoniae ompK^{evo}* versus wildtype. The volcano plots show the up- or downregulated proteins in all seven isolated *K. pneumoniae ompK^{evo}* clones. Cells were grown overnight in mGAM under anaerobic

1310 conditions and harvested after 20h for whole cell proteome analysis using mass spectrometry.

1311 Each strain was tested in three biological replicates.

1312

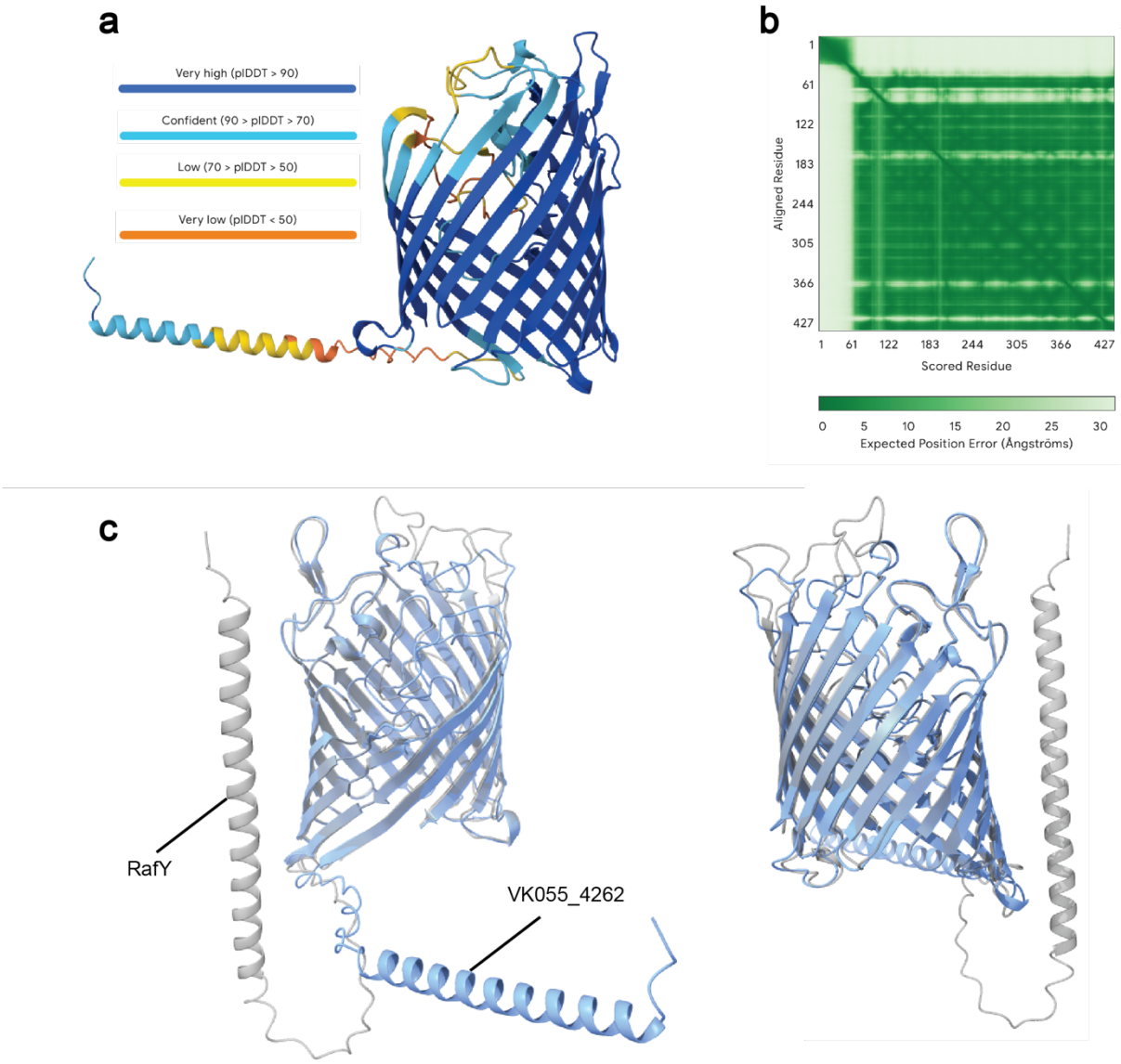

Extended Data Fig. 9: Structural prediction and comparisons for GlyP. a, AlphaFold prediction of the *K. pneumoniae* porin upregulated in *K. pneumoniae ompK*^{evo}. The AlphaFold-predicted structure of the mature protein (signal peptide removed) is shown as a cartoon representation colored by pLDDT confidence scores. The ß-barrel core is predicted with high confidence. **b**, Predicted aligned error (PAE) plot for the AlphaFold model. The PAE plot indicates high confidence in the relative positioning of residues withing the ß-barrel core, while increased PAE is primarily associated with extracellular loop regions. The short cytoplasmic helix also displays reduced confidence, consistent with local flexibility and disorder. **c,** Structure alignment of GlyP with RafY. UCSF ChimeraX structural superposition of the AlphaFold-predicted mature porin (blue) and RafY (grey) shows close alignment of the ß-barrel core with

divergence in loop regions. The alignment produced a sequence alignment score of 1495.9 and an RMSD of 0.67Å over 312 pruned atom pairs (22.3Å across all aligned residues).

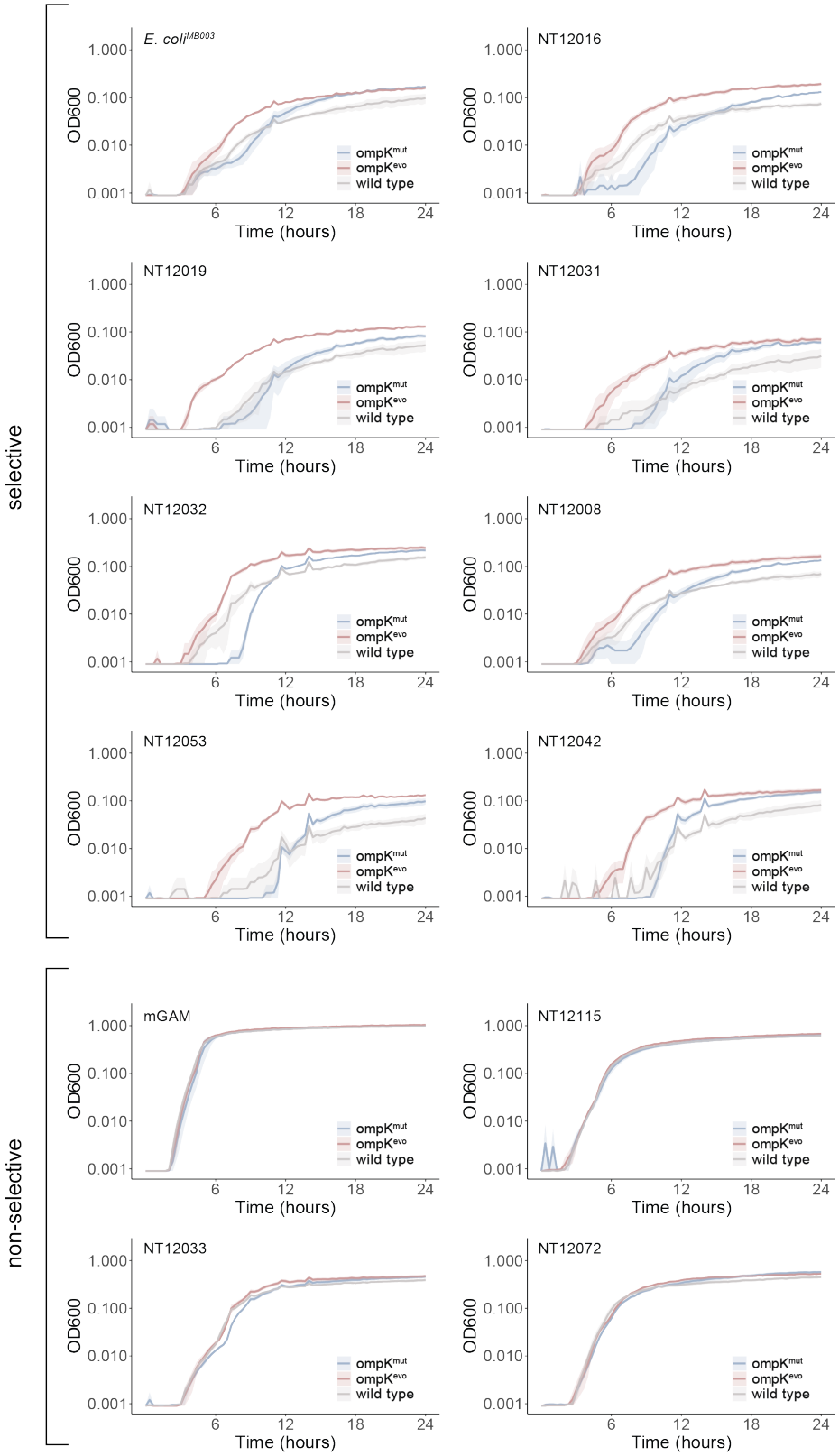

1327

1328 **Extended Data Fig. 10: Growth rates of *K. pneumoniae wildtype, ompK^{mut} and ompK^{evo}* in**
1329 **various *E. coli*-spent media.** The spent media were prepared by growing different *E. coli*
1330 strains overnight in mGAM at 37 ºC under anaerobic conditions and subsequent sterile

1331 filtration using a 0.22µM pore size filter. Lines represent average of four independent
1332 replicates, shades represent the standard deviation.
1333

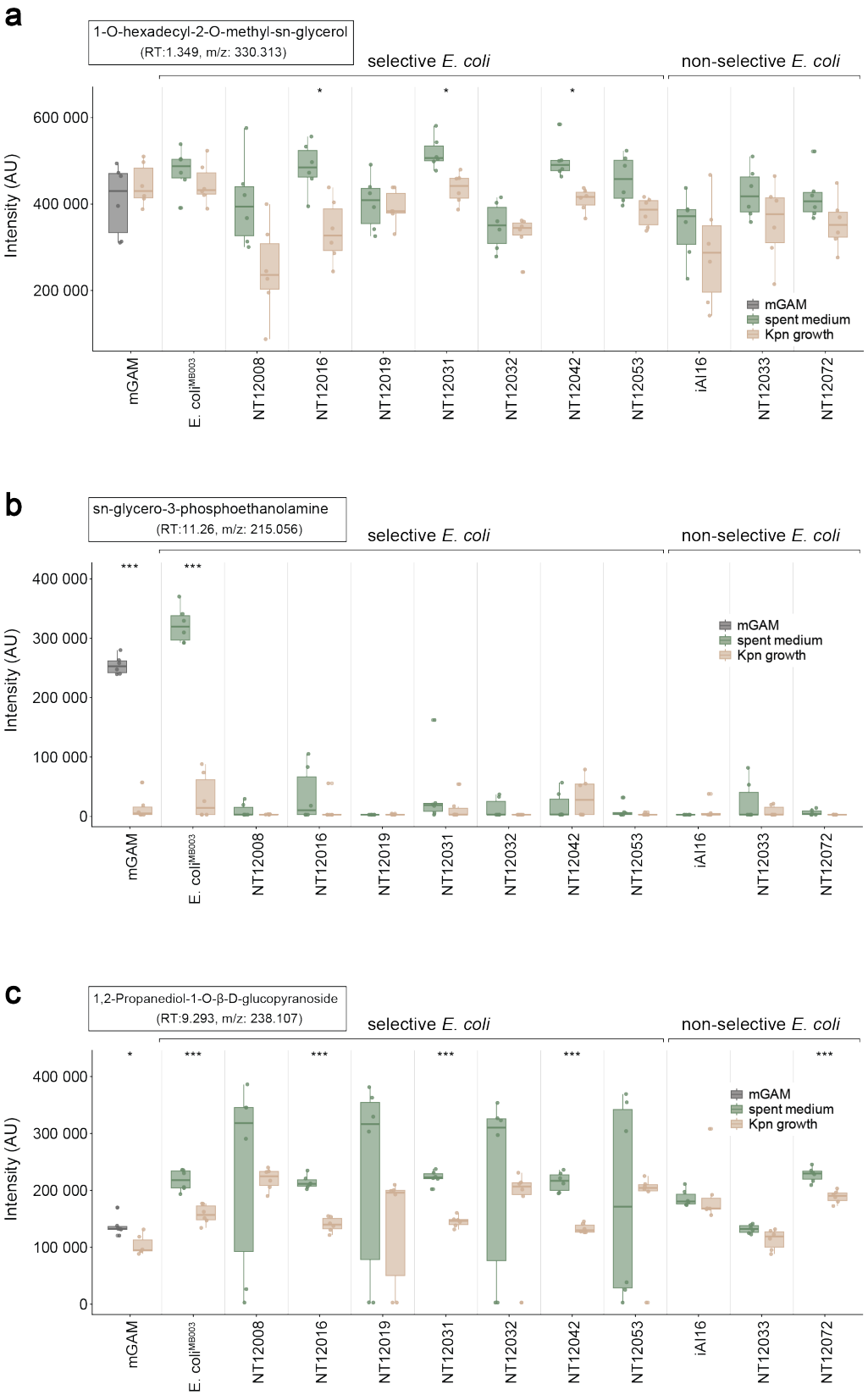

1334

1335 **Extended Data Fig. 11: Abundance of glycerol-containing metabolites in *E. coli*-spent media**
1336 **in the presence or absence of *K. pneumoniae*.** Absolute LC-MS signal intensities of (**a**) 1-O-
1337 hexadecyl-2-O-methyl-sn-glycerol (m/z 330.313), (**b**) sn-glycero-3-phosphoethanolamine

1338 (m/z 215.059) and (**c**) 1,2-Propanediol-1-O-β-D-glucopyranoside (m/z 238.107) in culture
1339 supernatants of *E. coli* before and after growth of *K. pneumoniae ompK*^{evo}. A reduction in
1340 signal intensity indicates depletion of these metabolites. Values are based on 6 biological
1341 replicates. Statistical significance was assessed using a t-test. * $p_{adjusted} < 0.05$, ** $p_{adjusted} <$
1342 0.01, *** $p_{adjusted} < 0.001$
1343